Research Square

Preprints are preliminary reports that have not undergone peer review.
They should not be considered conclusive, used to inform clinical practice,
or referenced by the media as validated information.

Research on the Long - term Surface Modification and Properties of Polyether Organosilicon Quaternary Ammonium Salts on Materials

Linfei Li
Taiyuan University of Science and Technology
Ran Wei
Taiyuan University of Science and Technology
Yimeng Zhao
Taiyuan University of Science and Technology
Lifei Zhi
lifeizhi@tyust.edu.cn
Taiyuan University of Science and Technology
Guoyong Wang
Taiyuan University of Science and Technology
Yongqiang Sun
North University of China

Research Article

Keywords: Polyether Silicone, Quaternary Ammonium Salt, Long-lasting Wetting, Long-lasting Antistatic Property, Long-lasting Antibacterial Activity

Posted Date: November 19th, 2026

DOI: https://doi.org/10.21203/rs.3.rs-11301407/v1

License: This work is licensed under a Creative Commons Attribution 4.0 International License.
Read Full License

Additional Declarations: No competing interests reported.

Research on the Long - term Surface Modification and Properties of Polyether Organosilicon Quaternary Ammonium Salts on Materials

Linfei Li[1], Ran Wei[1],Yimeng Zhao[1], Lifei Zhi*[1], Guoyong Wang[1], and Yongqiang Sun[2]

1 (College of Chemical Engineering and Technology, Taiyuan University of Science and Technology, Taiyuan 030024, P. R. China)

2 (College of Chemistry and Chemical Engineering, North University of China, Taiyuan 030051, P. R. China)

* Corresponding Author:

Lifei Zhi, College of Chemical Engineering and Technology, Taiyuan University of Science and Technology, Taiyuan 030024, P. R. China; Email: lifeizhi@tyust.edu.cn (L. Zhi); Tel: +8613068002395.

Highlights

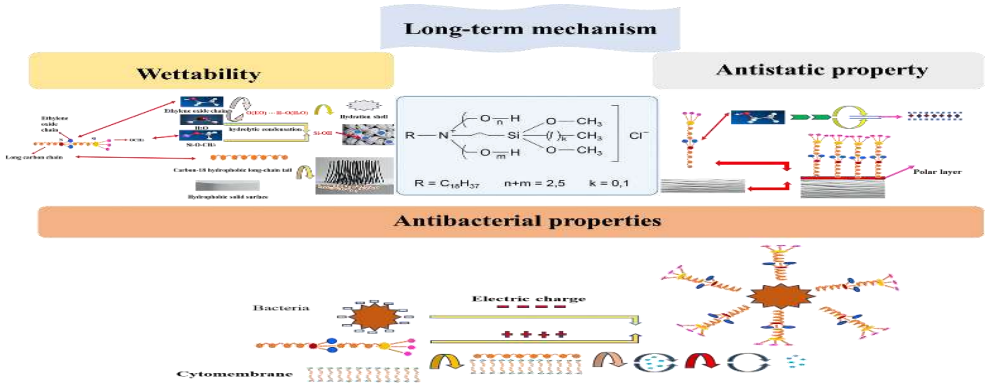
1. This paper reports for the first time that polyether siloxane quaternary ammonium salt surfactants can simultaneously possess three functions: long-acting

antibacterial activity, long-acting antistatic property and long-acting wettability.

2. This reaction features a straightforward synthetic route, where the target product can be obtained via a single-step quaternization process without generating any three wastes, and is readily scalable for industrial production.

3. Durable wettability (40 scrubs), antistatic (7 washes), and antibacterial (>99.9%) after 30 washes.

4. This product is non-toxic, non-irritating, and classified as an environmentally friendly surfactant.



Abstract

In high-end scenarios like functional coatings, medical textiles and electronic devices, simultaneously achieving durable antibacterial, wettability and antistatic properties has long been a core bottleneck in advanced material design, and no commercial product with this property combination is currently available on the market. Herein, four novel polyether siloxane quaternary ammonium surfactants

(2/3SiP2/5OPA) were synthesized via a one-step quaternization reaction using stearylamine polyoxyethylene ether (1802/1805) and 3-chloropropylmethyl di/tri-methoxysilane. Their chemical structures were verified via Fourier-transform infrared FT-IR and NMR. These surfactants exhibited excellent surface activity; notably, 3SiP2OPA achieved a cmc of 0.0031 g/L, while 2SiP2OPA reduced surface tension to 37.62 mN/m. TEM, DLS revealed hydrophobic-chain-dependent self-assembly into vesicles or spherical micelles with nano-scale bimodal distributions, alongside superior foam stability. Functional application tests demonstrate that the corn starch-based material modified by 2/3SiP2/5OPA exhibits excellent long-term wettability, withstanding up to 40 scrubbing cycles; after modification of polyurethane fabric, 2/3SiP2OPA outperforms 2/3SiP5OPA significantly in terms of antistatic durability (withstanding up to 7 washing cycles) and long-term antibacterial rate against Escherichia coli and Staphylococcus aureus (>99.9% after 30 washing cycles), which is attributed to its stronger interfacial chemical bonding capacity, verified by SEM and AFM. Furthermore, 3SiP2OPA exhibited enhanced softness (P-values: 1.26, 1.45 vs. standards) and was classified as non-toxic and non-irritating via cytotoxicity assays. This study demonstrates that the synthesized polyether silicone quaternary ammonium salt surfactant is a multifunctional environment-friendly product integrating non-toxicity, non-irritation, long-acting antibacterial property, long-acting wettability and long-acting antistatic performance, with great industrialization potential.

Keywords: Polyether Silicone; Quaternary Ammonium Salt; Long-lasting Wetting; Long-lasting Antistatic Property; Long-lasting Antibacterial Activity

1. Introduction

In high-end application scenarios including medical textiles, hygienic protective clothing, precision electronic packaging, and functional architectural coatings, the sustained pursuit of high-performance interfaces has increasingly centered on three critical yet typically mutually exclusive surface properties: strong long-lasting antibacterial activity, durable hydrophilic wettability, and long-term antistatic performance. In clinical environments, the persistent prevalence of healthcare-associated infections underscores an urgent need for surface modification technologies that can enable materials to maintain sustained bactericidal activity following repeated disinfection cleaning and mechanical abrasion. Concurrently, in the fields of smart materials and filtration membranes, wettability failure induced by the degradation of surface hydration layers represents a core bottleneck restricting their service life. The majority of existing commercially available modified products are restricted to single-functional additives, and currently no commercial product can simultaneously achieve all three properties. Traditional quaternary ammonium compounds, which are the mainstream of antibacterial treatment, face core challenges such as sharp declines in efficacy, elevated costs, and prevention and control failure with increasing cycles of use. Accordingly, long-acting bactericidal and disinfection products have become an inevitable rigid requirement for the industry to break through existing prevention bottlenecks and achieve cost reduction and efficiency improvement [1-3].

Long-acting bactericides offer the advantages of eliminating repeated operational steps, sustained active release, and low irritation. Furthermore, consumers now regard

antibacterial and anti-mite properties as core requirements when purchasing daily necessities, apparel, bedding, and upholstered furniture; meanwhile, surgical instrument coatings, medical textiles, and hospital architectural wall materials all impose stringent requirements for long-acting antibacterial performance. Nevertheless, most protective surfactants currently available on the market fail to achieve sustained long-term protection or exhibit suboptimal protective efficacy.

The term "long - acting property" describes the ability of a surfactant to retain its biological activity for an extended period after application [4]. Its working mechanism relies on the formation of a durable, stable functional interfacial layer on the substrate surface via chemical bonding of the surfactant. This structure can not only withstand repeated washing, friction, and erosion from various complex environments, but also continuously release active components with antibacterial and antistatic activities during dynamic application, thus achieving truly durable protection [5, 6].

Surfactants are involved in all aspects of daily human life, so it is commonly expected that they can achieve convenient operation, efficient long-term sterilization, and integrate multiple functions such as safety and environmental compatibility, non-toxicity, low irritation, softness, long-acting antistatic performance, and long-lasting wettability. This has imposed higher requirements for the development of multifunctional single-molecule surfactants. The molecular structure of a surfactant largely determines the physicochemical properties and application performance of the final product; therefore, the development of novel surfactants with optimized structures that integrate multiple functions simultaneously has become a cutting-edge research

hotspot in the field.

Traditional cationic surfactants exhibit weak intermolecular electrostatic repulsion and generally have a single hydrophobic chain structure [6-9]; the interfacial film they form at the gas-liquid interface has sufficient rigidity but insufficient flexibility, resulting in substantially lower foam stability compared to anionic surfactant systems [10]. Cationic organosilicon surfactants combine the low surface energy and flexibility of organosilicon structures with the cationic sterilization property of quaternary ammonium salts. The silyl groups in their molecular structure endow the molecules with characteristic organosilicon properties including ultra-low surface tension, excellent wetting and spreading performance, emulsifying capacity, and flexibility [11-13], while retaining the antibacterial and antistatic functions of quaternary ammonium salts. Moreover, leveraging the characteristic reaction between siloxane groups and material surfaces to form stable covalent bonds, this class of surfactants overcomes the limitation that traditional cationic surfactants, which rely only on physical adsorption, can hardly achieve long-acting antibacterial performance, and exhibits excellent washing resistance, abrasion resistance, and durable antibacterial efficacy [14] .

In this work, four polyether - based organosilicon quaternary ammonium salts (denoted 3/2SiP2/5OPA) were synthesized via a one-step quaternization reaction using octadecylamine polyoxyethylene ether (1802/1805) and 3-chloropropyl methyl di/trimethoxysilane as raw materials (Fig. 1). Their chemical structures were characterized via FT-IR and NMR spectroscopy. We achieved structural regulation and long-acting surface modification of the polyether organosilicon quaternary ammonium

salts, and conducted an in-depth investigation of their physicochemical properties, application performance, and long-acting mechanism performance.

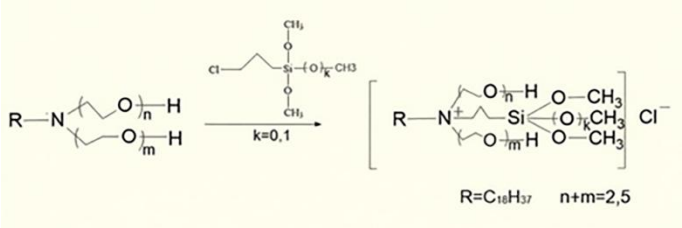


Fig. 1. Synthetic route of polyether-based silicone quaternary ammonium salt surfactant

2. Experiments

2.1. Materials

Octadecylamine polyoxyethylene ether (2 EO adduct, 1802, purity ≥99.9%) and octadecylamine polyoxyethylene ether (5 EO adduct, 1805, purity ≥99.9%) were purchased from Jiangsu Haian Petrochemical Plant; anhydrous ethanol and anhydrous disodium phosphate were obtained from Tianjin Zhiyuan Chemical Reagent Co., Ltd.; potassium dihydrogen phosphate (analytical grade) was supplied by Tianjin Chemical Reagent Wholesale Company; nutrient broth and nutrient agar medium were provided by Guangdong Huankai Microbial Technology Co., Ltd.; dodecyl dimethyl benzyl ammonium chloride (1227, mass fraction w=99%) and 3-chloropropyl methyl dimethoxysilane (purity 97%) were acquired from Shanghai Macklin Biochemical Technology Co., Ltd.; 3-chloropropyl trimethoxysilane (purity 98%) was procured from Shandong Guike New Materials Co., Ltd.; Anhydrous ether, analytical grade, was from Guoyao Group Chemical Reagent Co., Ltd.

Fourier transform infrared spectrometer, model VERTEX 70, supplied by Bruker

Corporation, Germany; nuclear magnetic resonance spectrometer, model AVANCE III, supplied by Bruker Corporation, Germany; electric blast drying oven, model 101-2ASB, supplied by Beijing Kewei Yongxing Instruments Co., Ltd.; automatic surface tensiometer, model KRÜSS-Tensiio, supplied by Krüss Scientific Instruments (Shanghai) Co., Ltd.; automatic drop shape analyzer, model KRÜSS-DSA25, supplied by Krüss Scientific Instruments (Shanghai) Co., Ltd.; foam analyzer, model FOAMSCAN, supplied by Teclis Instruments, France; nanoparticle size and zeta potential analyzer, model BeNano 90Zeta, supplied by Dandong Better Instruments Co., Ltd.; JEM-F200 transmission electron microscope, supplied by JEOL Ltd., Japan; RE-52AA rotary evaporator, manufactured by Shanghai Yarong Biochemical Instrument Factory; SXHT-250KJ rapid-open mechanical stirring reactor, manufactured by Shanghai Huotong Experimental Instrument Co., Ltd.； digital ultra-high resistance meter (PC68), from Shanghai Sixth Electric Meter Factory Co., Ltd.

2.2. 2SiP2/5OPA, 3SiP2/5OPA Synthesis Methods

A total of 48.03 g octadecylamine polyoxyethylene ether (2), 27.22 g 3-chloropropyltrimethoxysilane (for the synthesis of 3SiP2OPA) /26.56 g 3-chloropropylmethyldimethoxysilane (for the synthesis of 2SiP2OPA), and 50 g (for the synthesis of 3SiP2OPA) / 49.2 g (for the synthesis of 2SiP2OPA) ethanol were added into a high-pressure autoclave. The quaternization reaction was carried out at a stirring speed of 400 rpm and a reaction temperature of 180 °C. After 9 hours of reaction, the mixture was cooled naturally to room temperature. Ethanol was removed from the cooled mixture via reduced-pressure rotary evaporation to obtain the crude product.

The crude product was purified by washing three times with diethyl ether, followed by vacuum drying to afford the final products: 2SiP2OPA is N-polyoxyethylene ether (2)-1-octadecy-l-3-propylmethyldimethoxysilyl ammonium chloride, obtained as a white solid; 3SiP2OPA is N-polyoxyethylene ether (2)-1-octadecy-l-3-propyltrimethoxysilyl ammonium chloride, obtained as a pale yellow solid.

Octadecylamine polyoxyethylene ether (5) (53.72 g), 3-chloropropyltrimethoxysilane (22.02 g) or 3-chloropropylmethyldimethoxysilane (21.48 g), along with ethanol (50 g for the former reaction and 49.35 g for the latter reaction) were charged into a high-pressure autoclave. Quaternization reaction was conducted at a stirring rate of 400 r/min and a reaction temperature of 180℃. After reacting for 12 hours, the reaction mixture was allowed to stand and cool to room temperature. Ethanol was removed from the cooled mixture via reduced-pressure rotary evaporation to obtain the crude product. The crude product was purified by washing with diethyl ether three times, followed by vacuum drying, to yield a light yellow liquid product, namely N-polyoxyethylene ether (5)-1-octadecy-l-3-propylmethyldimethoxysilyl ammonium chloride (2SiP5OPA) and N-polyoxyethylene ether (5)-1-octadecy-l-3-propyltrimethoxysilyl ammonium chloride (3SiP5OPA), respectively.

2.3. Characterization of 2SiP2/5OPA and 3SiP2/5OPA

Raw materials including 1802, 1805, 3-chloropropyltrimethoxysilane and 3-chloropropylmethyldimethoxysilane, along with the as-synthesized products

2SiP2/5OPA and 3SiP2/5OPA, were loaded onto the instrument's sample stage and scanned in the wavenumber range of 4000-400 cm^{-1}. The structures of the obtained products were identified via Fourier-transform infrared spectroscopy by analyzing the characteristic absorption peaks corresponding to each functional group. Subsequently, ^{1}H nuclear magnetic resonance (^{1}H-NMR) and ^{13}C nuclear magnetic resonance (^{13}C-NMR) characterizations were performed on the synthesized products using a Bruker Avance III HD 500 MHz nuclear magnetic resonance spectrometer to confirm the molecular structures of the target compounds.

2.4. Surface Tension

The equilibrium surface tension of 2SiP2/5OPA, 3SiP2/5OPA and 1227 was measured via the platinum ring method using a Hamburg KRÜSS-Tiniio automatic surface tensiometer manufactured in Germany. Deionized water was used as the solvent, and aqueous solutions with uniform concentration gradients were prepared for each test sample to ensure complete dissolution and homogeneity of the resulting solutions. All measurements were performed at a controlled temperature of 25±0.1℃, and the instrument was calibrated with standard solutions prior to measurement [15].

2.5. Dynamic Surface Tension

At a constant temperature of 25 °C ± 0.1 °C, the dynamic surface tension of aqueous solutions containing 2SiP2/5OPA, 3SiP2/5OPA and 1227 with uniform concentration gradients was directly measured via a fully automatic drop shape tensiometer, after which the experimental data were recorded and processed.

2.6. Transmission Electron Microscopy

The structures of 2SiP2/5OPA and 3SiP2/5OPA aggregates were characterized using a JEM-F200 field emission electron microscope via negative staining [16]. Briefly, the sample was placed on a copper grid for 5 minutes, blotted dry with filter paper, then stained with 2 wt% sodium phosphotungstate for 15 minutes. All prepared samples were stored at room temperature for at least 2 hours prior to measurement, and the concentration of each experimental sample was adjusted to 10 g/L.

2.7. Dynamic Light Scattering

Measurements were performed using a nanoparticle size and zeta potential analyzer, Model BeNano 90Zeta. Solutions of 2SiP2/5OPA and 3SiP2/5OPA at different concentrations were prepared in advance and allowed to stand for a period of time to reach a stable state. Subsequently, at a constant temperature of 25℃, 1-2 mL of the prepared solution was transferred to a designated analytical test tube, and the tube was placed into the sample cell for measurement [17, 18].

2.8. Morphological Characterization of Foams

In this work, foam stability was characterized via the gas sparging method using a FOAMSCAN foam analyzer (Teclis, France). The concentrations of the 2SiP2/5OPA, 3SiP2/5OPA, and 1227 sample solutions were set as 0.1 g/L, 0.5 g/L, 1 g/L, 5 g/L, and 10 g/L respectively, while the gas flow rate was held constant at 150 mL/min. The initial foam volume was standardized to 180 mL. Throughout the 1000-second measurement duration, variations in foam volume and morphology were monitored systematically.

After the test sample was slowly injected into the designated test tube, the sample chamber was sealed prior to measurement, following which the collected test data were processed and analyzed [19].

2.9. Study on Long-Term Wettability of Modified Corn Starch-Based Degradable Materials

This test was conducted via the sessile drop method using a fully automatic water drop shape analyzer. First, 2SiP2/5OPA and 3SiP2/5OPA solutions with a concentration of 2 g/L were prepared using ultrapure water. The material was then cut into 3×3 cm fragments under constant temperature and humidity conditions (25℃, 50% RH). The static water contact angle on the surface of the untreated material was measured first, after which the aqueous solution of the product was sprayed onto the material surface for modification. The contact angle of the modified material was measured again after drying in atmospheric conditions. To test the long-term stability of the wetting effect after modification, repeated wiping-drying cycles were performed on the treated samples, and the variation trend of the contact angle was further investigated [20, 21] .

2.10. Flexibility Test

The softness test is performed in compliance with the relevant specifications of GB/T 13174-2021. First, pure cotton white cloth is boiled with a detergent, rinsed with deionized water until the pH reaches neutral, dried and ironed, then cut into 10 cm × 10 cm fabric specimens for subsequent use. Next, 50 mg/kg hard water, a 0.2% mass fraction sample solution and a standard detergent solution are prepared. Five test fabric

specimens are loaded for each test run, washed for 20 minutes, followed by two repeated rounds of rinsing and dehydration. The aforementioned washing cycle is carried out for a total of 5 rounds in a vertical decontamination tester. After the completion of all cycles, the fabric specimens are removed, rolled twice horizontally and twice vertically with a roller, and then air-dried for 24 hours. The treated fabric specimens are laid flat with the front side facing upward at the center of the test bench of the softness tester, after which the instrument is activated for measurement, and the measured values (retained to one decimal place) are recorded. After outliers are eliminated via the Q-test, the softness ratio P is calculated, and the sample is determined to have qualified softening performance when $P \geq 1.1$.

2.11. Evaluation of Long-Term Antistatic Performance

The test for durable antistatic performance is carried out in strict accordance with the national standard GB/T 16801-2013. First, cut the polyester fabric into test specimens with dimensions of 100 mm × 100 mm, then wash the specimens in a rinsing apparatus with a 1 g/L soap solution for 15 minutes. The washing procedure adopts alternating clockwise and counterclockwise rotation, with 5 cycles per rotation direction, where each rotation lasts 3 minutes followed by a 2-minute pause, and dehydration is performed immediately after washing. Subsequently, rinse the specimens three times with distilled water, with each rinse lasting 3 minutes, then dry the specimens at 45 ℃ for 4 hours. Finally, immerse the specimens in the sample solution for 10 minutes, dry them again, and place the treated specimens with a sheet of filter paper between adjacent specimens to avoid interference. After the pretreatment

is completed, a super-high resistance meter is employed to measure the surface resistance of the specimens. The antistatic performance is evaluated based on the variation of the specific surface resistance or its logarithm, and repeated tests are conducted to characterize the durable antistatic performance of the specimens.

2.12. Test for Long-term Antibacterial Performance

2.12.1. Viable Counting Method

First, the viable bacterial concentrations of Staphylococcus aureus (ATCC 6538) and Escherichia coli (ATCC 8099) were quantified to ensure the reliability and repeatability of subsequent antibacterial assay results. Resuscitated fresh bacterial suspensions were inoculated into nutrient broth and cultured with constant shaking at 37 °C. Via the ten-fold serial gradient dilution method, the bacterial suspensions were serially diluted with phosphate-buffered saline to obtain 7 concentration gradients ranging from 10^{-1} to 10^{-7}. For each dilution, 100 μL of bacterial suspension was pipetted onto the surface of a pre-prepared agar plate, and immediately uniformly spread with a disposable sterile spreading rod until the bacterial suspension was completely absorbed by the medium. After the plate surface dried, the plates were incubated statically in an inverted position in a 37 °C constant-temperature incubator for 24 hours. Upon completion of incubation, plates with colony counts between 30 and 300 CFU were selected for enumeration. Three parallel replicates were set for each dilution, and the average value was calculated to convert the result into the viable bacterial concentration (CFU/mL) of the original bacterial suspension. This calibration step provides a unified, accurate bacterial concentration benchmark for the subsequent long-term antibacterial durability testing of samples via the shaking method.

2.12.2. Test on Long-term Antibacterial Properties of Polyurethane Fabric After Sample

Modification

The oscillation method was utilized to characterize the long-term antibacterial performance of polyurethane fabrics modified with 2SiP2/5OPA and 3SiP2/5OPA. First, the polyurethane fabrics were cut into 10×10 mm fragments with a mass of 0.5 ± 0.05 g. The fragments were then immersed in 10 g/L 2SiP2/5OPA and 3SiP2/5OPA solutions respectively, and incubated in the dark for 12 h. After air-drying at room temperature, the fabric fragments were sealed in conical flasks for subsequent use. Before the experiment, all samples, pipettes, conical flasks and PBS buffer (pH 7.4) were sterilized via autoclaving at 121 °C and 103 kPa. A blank control group (45 mL PBS + 5 mL bacterial suspension) and an antibacterial test group (0.5 g fabric sample + 45 mL PBS + 5 mL bacterial suspension) were established, with three replicates per group. The concentrations of Staphylococcus aureus (ATCC 6538) and Escherichia coli (ATCC 8099) suspensions were adjusted to 1×10^4-5×10^4 CFU/mL. For the blank control group, after shaking at 250 rpm for 1 min, the bacterial suspension was spread on agar plates to quantify the initial bacterial count. For the antibacterial test group, after shaking incubation at 37 °C for 18 h, the bacterial suspension was serially diluted and spread on agar plates to count the number of surviving bacteria. After completing the initial antibacterial test, the fabric samples were collected for cyclic washing treatment: each washing cycle was conducted at a rotation speed of 960 rpm for 2 min, and cumulative washing cycles of 0, 1, 5, 10, 20 and 30 were set respectively. Corresponding fabric samples were collected at each washing node, and the bactericidal rate was measured repeatedly following the aforementioned antibacterial testing protocol to evaluate the

long-term antibacterial performance after different numbers of washing cycles.

2.12.3. SEM Measurement

Fabric sheet samples that underwent different numbers of washes via the oscillation method were first treated with gold sputtering, then placed in the sample chamber of a scanning electron microscope for morphological observation, alongside qualitative and semi-quantitative elemental analysis.

2.12.4. AFM Measurement

Fabric samples prepared via the oscillation method with different washing cycles were subjected to drying treatment, then uniformly mounted onto a rigid substrate using conductive adhesive. This protocol enables the acquisition and export of nanoscale topography and mechanical property data of the fiber surface for subsequent analysis.

2.12.5. Stimulation Experiments

Following the skin irritation test protocol outlined in Section 2.3.3 of the Disinfection Technical Specifications (2002 Edition), 3SiP2OPA was subjected to the aforementioned test, with the sample batch number designated as 2025SP14849R01.

2.12.6. Acute Oral Toxicity Test

According to the requirements for the acute oral toxicity test specified in Section 2.3.1 of the Disinfection Technical Specifications (2002 Edition), 3SiP2OPA (Batch No.: 2025SP14849R01) was tested.

3. Results and Discussion

3.1. Structural Characterization

The raw materials and products were characterized via FT - IR spectra, ^{1}H-NMR and ^{13}C-NMR.

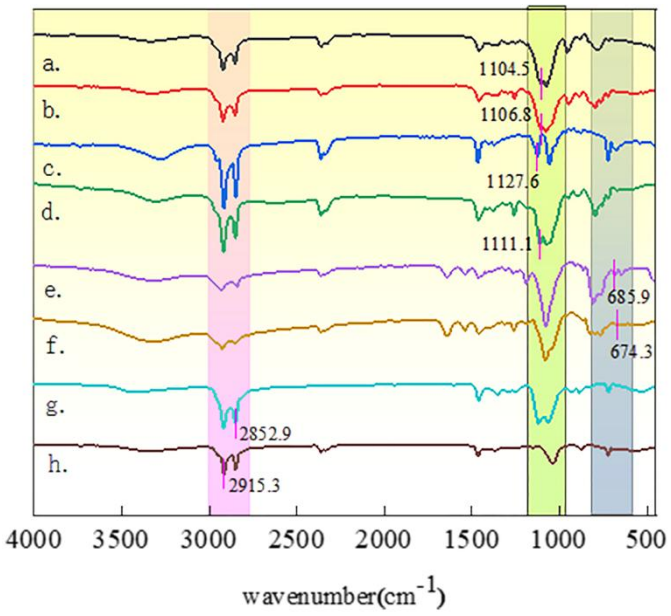


Fig. 2. the FT - IR spectra. (a) 3SIP5OPA, (b) 2SIP5OPA, (c) 3SIP2OPA, (d) 2SIP2OPA, (e) 3 - chloropropyltrimethoxysilane, (f) 3 - chloropropylmethyldimethoxysilane, (g) octadecylamine polyoxyethylene ether (5), (h) octadecylamine polyoxyethylene ether (2)

As illustrated in Fig. 2, the stretching vibration absorption peaks of -CH_3 and -CH_2 are located at 2915.3 cm^{-1} and 2852.9 cm^{-1}, respectively. The characteristic absorption peaks of quaternary ammonium salts are observed at 1104.5 cm^{-1}, 1106.8 cm^{-1}, 1127.6 cm^{-1} and 1111.1 cm^{-1}. Furthermore, in the present study, the C-Cl stretching vibration peaks at 674.3 cm^{-1} and 685.9 cm^{-1}, which are unique to 3-chloropropylmethyldimethoxysilane and 3-chloropropyltrimethoxysilane, are notably absent. This provides preliminary evidence confirming the successful synthesis of the target product.

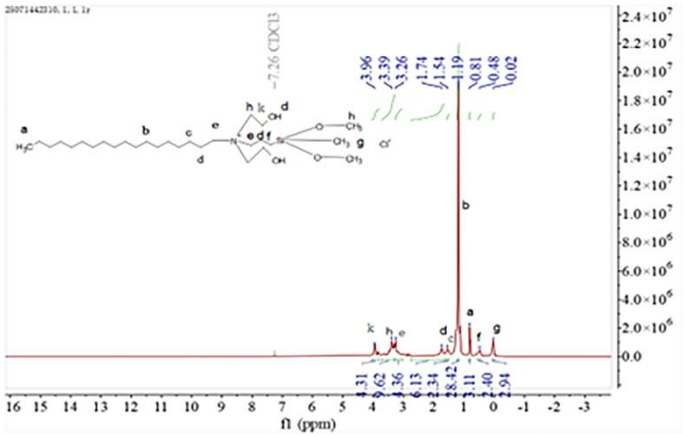


Fig. 3. ^{1}H NMR spectrum of 2SiP2OPA

2SiP2OPA: ^{1}H-NMR($CDCl_3$, ppm): δ: 0.02(s, 3H, $SiCH_3$), 0.48(t, 2H, $SiCH_2$), 0.81(t, 3H, CH_3), 1.19(m, 28H, $CH_2CH_2CH_2CH_2CH_2CH_2CH_2CH_2CH_2CH_2CH_2CH_2CH_2CH_2$), 1.54(m ,2H, CH_2), 1.74(m, 6H, CH_2, CH_2, 2OH), 3.26(m, 4H, $_2HCN+CH_2$), 3.39(t, 10H, $SiO((OCH_3)_2)$, $N+((CH_2)_2)$, 3.96(m, 4H, $(CH_2O)_2$).

3SiP2OPA: ^{1}H-NMR($CDCl_3$, ppm): δ: 0.60(t, 2H, SiCH2), 0.84(t, 3H, CH3), 1.22(m, 30H, CH2CH2CH2CH2CH2CH2CH2CH2CH2CH2CH2CH2CH2CH2CH2), 1.62(m, 4H, CH2CH2), 1.76(m, 2H, 2OH), 3.33(m, 4H, 2HCN+CH2), 3.67(t, 4H, N+((CH2)2), 3.86(m, 9H, Si(OCH3)3), 3.97(m, 4H, (CH2O)2).

2SiP5OPA: ^{1}H-NMR($CDCl_3$, ppm): δ: 0.54(t, 3H, $SiCH_2$), 0.86(t, 3H, CH_3), 1.23(m, 32H, $CH_2CH_2CH_2CH_2CH_2CH_2CH_2CH_2CH_2CH_2CH_2CH_2CH_2CH_2CH_2CH_2$), 3.35(m, 10H, $(CH_2O)_5$), 3.62(t, 6H, $SiO((OCH_3)_2)$).

3SiP5OPA: ^{1}H-NMR($CDCl_3$, ppm): δ: 0.89(t, 3H, CH_3), 1.25(m, 32H, $CH_2CH_2CH_2CH_2CH_2CH_2CH_2CH_2CH_2CH_2CH_2CH_2CH_2CH_2CH_2CH_2$), 3.38(m, 10H,

$(CH_2O)_5$), 3.64(t, 9H, $SiO((OCH_3)_3)$).

2SiP2OPA: ^{13}C-NMR ($CDCl_3$, ppm) : 0.78($SiCH_3$), 14.03(CH_2), 15.16(CH_3), 18.32($NSiCH_2$), 22.61(CH_2), 26.68(CH_2CH_2), 29.29($CH_2CH_2CH_2CH_2CH_2CH_2CH_2CH_2CH_2CH_2CH_2CH_2$), 31.86($CH_2$), 52.23($SiO(CH_3)_2$), 56.07($N+(CH_3)_2$), 65.95($N+CH_2$), 77.43($(CH_2O)_2$).

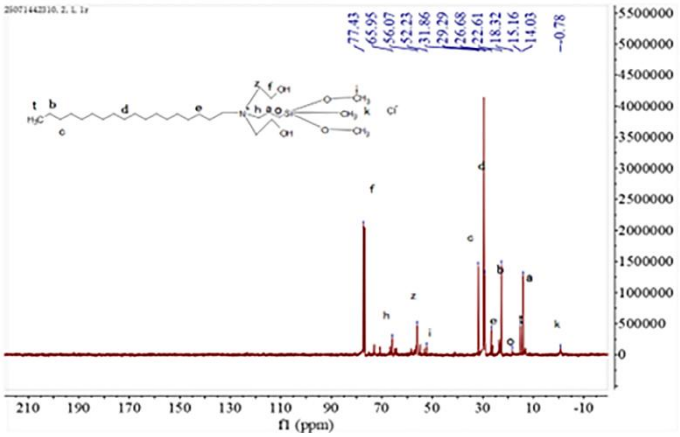


Fig. 4. ^{13}C NMR spectrum of 2SiP2OPA

3SiP2OPA: ^{13}C-NMR ($CDCl_3$, ppm) **:** 14.04(CH2), 15.17($SiCH_2$, CH3), 22.62(CH2), 26.15(CH2), 29.64(CH_2), 31.87(CH_2), 56.28($SiO(CH_3)_3$), 65.97($N+CH_2$), 66.74($N+CH_2$), 77.35($(CH_2O)_2$).

2SiP5OPA: ^{13}C-NMR ($CDCl_3$, ppm) : 14.12 (CH_3), 15.24($SiCH_2$), 22.69(CH_2),26.84(CH_2), 29.82($CH_2CH_2CH_2CH_2CH_2CH_2CH_2CH_2CH_2CH_2CH_2CH_2$), 31.92($CH_2$), 61.51($Si(OCH_3)_2$, $(CH_2O)_5$), 72.67($N+(CH_3)_2$), 77.31($(N+CH_2)_5$).

3SiP5OPA: ^{13}C-NMR ($CDCl_3$, ppm) : 14.12(CH_3), 18.29(CH_2), 23.05(CH_2), 26.87(CH_2), 29.71($CH_2CH_2CH_2CH_2CH_2CH_2CH_2CH_2CH_2CH_2CH_2CH_2$), 31.92($CH_2$),53.22($Si(OCH_3)_3$, $((CH_2O)_5)$), 73.08($N+CH_2$), 77.05($N+CH_2$).

As presented in Fig. 3, the ^{1}H-NMR spectrum of 2SiP2OPA is illustrated, and Fig. 4 displays the ^{13}C-NMR spectrum of the same compound. (Full ^{1}H-NMR and ^{13}C-NMR data for 3SiP2OPA, 2SiP5OPA, and 3SiP5OPA are provided in the Supporting Information S1-S6) In the ^{1}H-NMR spectrum (Fig. 3), the signals observed at 3.39 ppm, 3.86 ppm, 3.62 ppm, and 3.64 ppm are assigned to the characteristic resonance of quaternary ammonium salt, confirming the successful synthesis of the target product. The structure of the product was further verified via FT-IR, ^{1}H-NMR, and ^{13}C-NMR analyses. The proposed synthetic route features concise operation and high efficiency, is free of hazardous three-waste emission, can realize engineering scale-up with conventional existing production equipment, and satisfies the requirements of green industrial manufacturing.

3.2. Surface Tension

The experimental results demonstrate that prior to reaching the critical micelle concentration (CMC), the surface tension of the solution decreases linearly with increasing surfactant concentration. This phenomenon can be attributed to the gradual formation of ordered arrangements of surfactant molecules at the interface. Upon reaching the critical micelle concentration, the curve exhibits an abrupt change. As the surfactant concentration continues to increase, the response of the solution's surface tension on the equilibrium surface tension curve (γ-logc curve) diminishes (Fig. 5). The surface adsorption parameters were determined via the simplified Gibbs adsorption isotherm (Equation 1 and Equation 2). The standard Gibbs free energy of adsorption and the standard Gibbs free energy of micellization in aqueous solution (ΔG^{θ}_{ads} and

ΔG^{θ}_{mic})were calculated via Equation 3 and Equation 4, respectively [22, 23] .

$$\Gamma_{max} = \frac{-1}{2.303nRT} \left(\frac{\partial \gamma}{\partial log c}\right)_T \quad (1)$$

$$A_{min} = \frac{1}{N A \Gamma max} \quad (2)$$

$$\Delta G^{\theta}_{ads} = nRT\ln\left(\frac{CMC}{\alpha}\right) - 6.022\pi A_{min} \quad (3)$$

$$\Delta G^{\theta}_{mic} = nRT\ln\left(\frac{CMC}{\alpha}\right) \quad (4)$$

For the cationic surfactants employed in this study, the aggregation number n is set to 2. In the aforementioned expression, α represents the molar concentration of water (55.3 mol· L^{-1} at 25 °C), R denotes the universal molar gas constant (8.314 $J \cdot mol^{-1} \cdot K^{-1}$), T is the absolute temperature in Kelvin, N_A corresponds to Avogadro's constant (6.022×10^{23} mol^{-1}), and $\pi = \gamma_0 - \gamma CMC$ is defined as the surface pressure at the saturated adsorption interface, where γ_0 refers to the surface tension of pure water (72 mN/m at 25 °C). At 25 °C, the maximum surface excess concentration (Γ/m^2) is calculated based on the "molar maximum" framework, and the calculated values of all characteristic surface activity parameters are summarized in Table 1.

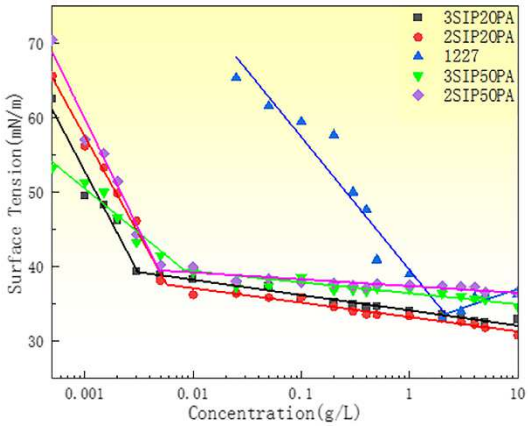


Fig. 5. Surface tension versus concentration curves for 3SiP2OPA, 2SiP2OPA, 3SiP5OPA, 2SiP5OPA and 1227

Dodecyl dimethyl benzyl ammonium chloride (1227) is currently the quaternary ammonium cationic surfactant with the largest production volume, widest range of applications, and most mature industrial chain among commercial products of this category. However, long-term widespread application has enabled bacteria and fungi to develop exponentially increasing resistance to 1227 via continuous gene mutation or exogenous gene integration [24, 25], For this reason, 1227 was selected as the control sample for performance comparison with 2SiP2/5OPA and 3SiP2/5OPA. As illustrated in Figure 5, at equal concentrations, both 2SiP2/5OPA and 3SiP2/5OPA exhibit lower surface tension than 1227, and 1227 shows higher surface tension than 2SiP2/5OPA and 3SiP2/5OPA at identical concentrations in most cases. This phenomenon can be ascribed to the excess interfacial adsorption induced by the amphiphilic structure formed via ethylene oxide polymerization in the long carbon chain. When 2SiP2/5OPA and 3SiP2/5OPA are dissolved in aqueous solution, the C_{18} hydrophobic tails spontaneously migrate to the air-water interface driven by the hydrophobic effect of water, with the alkyl chains oriented toward the air phase. Simultaneously, the $(EO)_mH$

hydrophilic head groups anchor in the subsurface water layer through ether oxygen hydration, forming a monomolecular adsorption layer with controllable density. This adsorption layer replaces high-energy interfacial water molecules with low-surface-energy -CH_3/-CH_2- segments, thereby reducing the interfacial free energy density and ultimately leading to a reduction in surface tension [22, 26]. The surface tension of 3/2SiP5OPA is higher than that of 3/2SiP2OPA because 3/2SiP5OPA contains more polymerized ethylene oxide units. Elongation of the EO chain increases the hydrophilic volume of the molecule and the thickness of the hydration layer, which relatively weakens the thermodynamic driving force for hydrophobic association to form micelles. Consequently, a higher bulk concentration is required to trigger micellization, resulting in an increase in the critical micelle concentration (CMC) [27]. The surface tension of 2SiP2/5OPA and 3SiP2/5OPA continues to decrease gradually with increasing concentration, which may be associated with a multi-step adsorption mechanism: the synthesized surfactant molecules may undergo further rearrangement at the interface or form additional adsorption layers at high concentrations, leading to a further reduction in surface tension. The increase in the surface tension of 1227 after reaching the critical micelle concentration (CMC) can be attributed to the fact that the 1227 employed in this experiment is an industrial product containing trace amounts of homologous impurities, including free amines and long-chain alcohols. When the bulk concentration exceeds the CMC, these impurities are solubilized within micelles and competitively displaced from the interface, leading to a slight increase in the apparent surface tension after it reaches the minimum value.

Table 1 Surface adsorption and aggregation parameters of different Samples in aqueous solution

Surfactant	CMC (g/L)	γCMC (mN/m)	Γmax (mol/cm^{-2})	Amin(Å^2)	ΔG^{Θ} ads (kJ/mol)	ΔG^{Θ} mic (kJ/mol)
3SIP2OPA	0.0031	39.38	2.40×10 $^{-10}$	69.21	-93.49	-79.89
2SIP2OPA	0.0057	37.62	2.32×10 $^{-10}$	71.60	-94.71	-76.74
3SIP5OPA	0.007	39.75	1.12×10 $^{-10}$	148.32	-105.75	-76.94
2SIP5OPA	0.0048	39.53	2.61×10 $^{-10}$	63.64	-92.33	-78.68
1227	2.161	33.69	1.56×10 $^{-10}$	106.48	-104.46	-44.98

As illustrated in Table 1, a comparison of five distinct surfactants reveals that the critical micelle concentration (CMC) of cationic surfactant 1227 is 2.161 g/L, while the CMC values of 2SiP2/5OPA and 3SiP2/5OPA are 0.0057 g/L, 0.0048 g/L, 0.0031 g/L, and 0.0007 g/ L, respectively, all of which are substantially lower than that of 1227. This observation can be attributed to two contributing factors:1. Chain length effect: the carbon chain length of 3/2SiP2OPA and 3/2SiP5OPA is six CH_2 units longer than that of 1227, leading to a significantly higher CMC for 1227 relative to the four surfactants [22]. 2. Electrostatic repulsion of ionic head groups: the positively charged N^+ groups on the micelle surface of 1227 experience mutual electrostatic repulsion. To stabilize the micellar structure, 1227 reduces repulsion by limiting packing density, tends to form aggregates with larger aggregation numbers, and achieves charge neutralization partially via counterions (Cl^-). In contrast, the head groups of 2SiP2/5OPA and 3SiP2/5OPA are surrounded by electrically neutral EO hydration shells; the primary factors inhibiting micellization in these surfactants are the conformational entropy loss of EO chains and the steric hindrance of EO hydration layers [28, 29]. The combined effect of these two factors results in CMC values for

2SiP2/5OPA and 3SiP2/5OPA that are substantially lower than that of 1227.

Furthermore, the Γmax of 2SiP2/5OPA and 3SiP2/5OPA is generally higher than that of 1227, which can be ascribed to their smaller hydrophilic head groups relative to 1227, enabling tighter ordered packing at the interface. The minimum cross-sectional area per molecule of 2SiP2/5OPA and 3SiP2/5OPA is overall smaller than that of 1227, since 1227 contains a bulky rigid benzyl moiety and its quaternary ammonium head group is surrounded by an extended hydration layer, resulting in a larger interfacial footprint and relatively loose packing. In contrast, the flexible EO chains in 2SiP2/5OPA and 3SiP2/5OPA allow surfactant molecules to adopt more compact conformations, thereby achieving higher effective interfacial coverage. The experimental results demonstrate that both ΔG^{θ}_{ads} and ΔG^{θ}_{mic} are negative, confirming that the adsorption and micellization processes are thermodynamically spontaneous. The relative magnitude of the free energy changes ($|\Delta G^{\theta}_{ads}| > |\Delta G^{\theta}_{mic}|$) indicates that these surfactants have a higher thermodynamic tendency to adsorb at interfaces than to form micelles in aqueous solution [15, 30, 31].

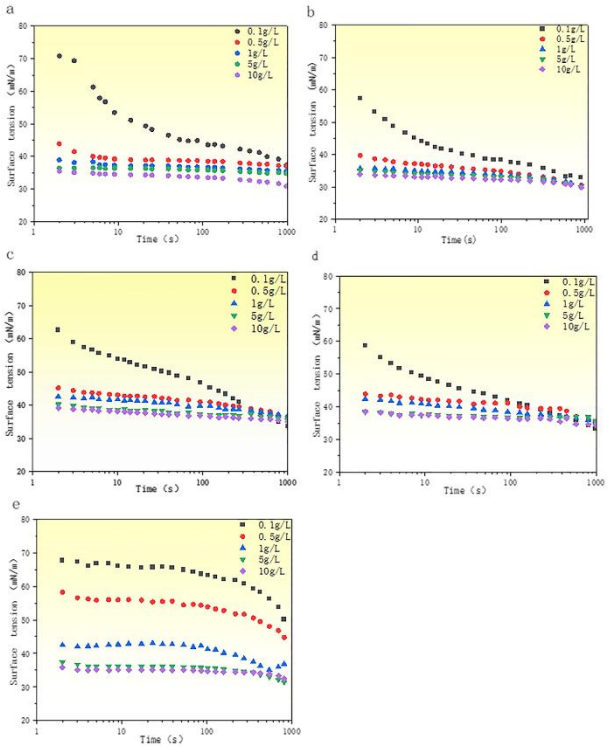


Fig. 6. Dynamic surface tension of different surfactant solutions at varied concentrations. (a) 3SiP2OPA, (b) 2SiP2OPA, (c) 3SiP5OPA, (d) 2SiP5OPA, (e) 1227

As shown in Fig. 6, dynamic surface tension is defined as the relationship between surface tension and time, which reflects the adsorption rate of surfactant molecules transferring from the bulk phase to the interface. The dynamic surface tension profile can be divided into four regions: the induction region, the rapid decay region, the mesoequilibrium region and the equilibrium region. For all tested samples, the dynamic surface tension curves exhibit a downward trend with increasing concentration, accompanied by reduced decay amplitude and rate, gradual narrowing of the induction region, and earlier emergence of the rapid decay region. This phenomenon is attributed to the increase in concentration gradient in the bulk phase and the consequent rise in molecular diffusion flux with increasing concentration, which leads to a rapid decrease in surface tension. However, as the concentration continues to increase and approaches

or exceeds the critical micelle concentration (CMC), the surface adsorption sites gradually become saturated. At this stage, although molecules arrive at the surface extremely rapidly, the increased steric hindrance in the surface layer makes it difficult for newly arrived molecules to arrange more tightly to reduce surface energy. As a result, the decay amplitude (slope) of the late-stage curve gradually decreases and levels off. At a low concentration of 0.1 g/L, 2SiP2/5OPA and 3SiP2/5OPA enter the rapid decay region within 2 seconds, and reach the equilibrium region before 1227 enters the rapid decay region, with a considerable decay magnitude. When the concentration increases to 0.5 g/L, 2SiP2/5OPA and 3SiP2/5OPA basically reach the equilibrium region at the initial stage, while 1227 only enters the rapid decay region after 216 seconds. The reason for this observation is that the hydration of polymerized ethylene oxide in 2SiP2/5OPA and 3SiP2/5OPA delays the initial adsorption. However, at high concentrations, the flexibility of the EO chain allows molecules to undergo late-stage rearrangement more rapidly, thus reaching a lower equilibrium surface tension within a shorter time[22, 26] .

3.3. Aggregation Behavior in Aqueous Solutions

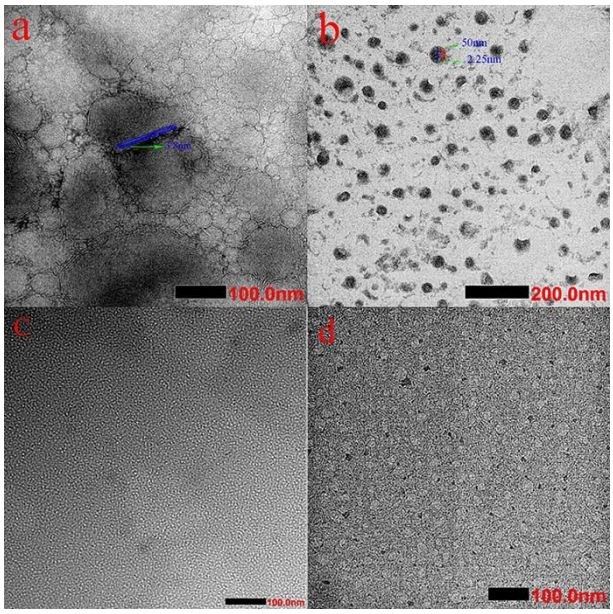


Fig. 7. Transmission electron microscopy images of different samples at a concentration of 10 g/L. (a) 3SiP2OPA, (b) 2SiP2OPA, (c) 3SiP5OPA, (d) 2SiP5OPA

As demonstrated in Fig. 7, the micromorphology characterized by transmission electron microscopy (TEM) reveals that 2/3SiP2OPA adopts a layer-by-layer encapsulated vesicle structure.(The enlarged images of the samples are presented in the Supporting Information S7-S10) This structural characteristic is most likely attributed to the overly long C_{18} carbon chain of 2/3SiP2OPA, which induces an exponential increase in hydrophobicity. To fully shield this long hydrophobic tail, molecules are required to pack tightly side-by-side and assemble into a dense bilayer membrane analogous to biological cell membranes. In comparison, 2/3SiP5OPA forms a uniformly dispersed spherical micelle structure. This distinct morphology can be attributed to the high number of polymerized ethylene oxide units (five ethylene oxide units) in its C_{18} carbon chain, which generates substantial internal steric hindrance during carbon chain aggregation.

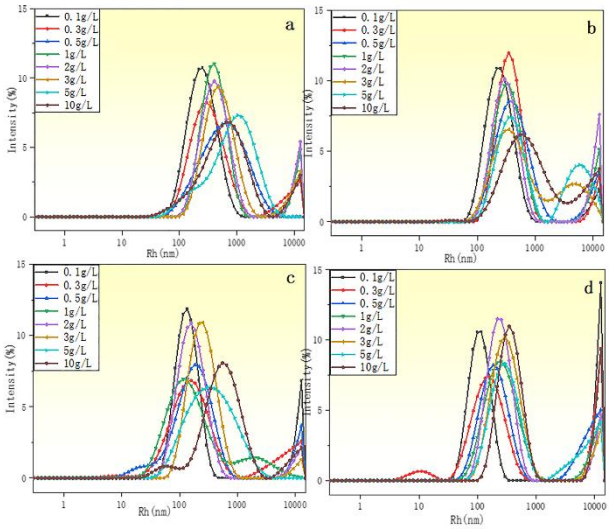


Fig. 8. Intensity-weighted particle size distributions at different concentrations (a) 3SiP2OPA, (b) 2SiP2OPA, (c) 3SiP5OPA, (d) 2SiP5OPA

Fig. 8 presents the dynamic light scattering (DLS) particle size distribution results of 2SiP2/5OPA and 3SiP2/5OPA. The results demonstrate that the aggregates exhibit a bimodal size distribution at the nanometer scale. For 2SiP2/5OPA and 3SiP2/5OPA in the low-concentration region (0.1 g/L-0.5 g/L), the intensity of the scattering peak decreases significantly with increasing concentration, shifts toward a larger hydrodynamic radius (R_h), and the peak shape becomes broader. In the medium - concentration region (1 g/L-3 g/L), the scattering peak intensity increases and the peak shape becomes sharper. In the high - concentration region (5 g/L-10 g/L), the intensity of the main peak decreases sharply again and the peak shape broadens once more. This phenomenon arises because at low concentrations, a small number of C_{18} tails pair via hydrophobic effects, leading to two to several molecules sharing a single hydrophobic microdomain; the resulting assemblies are dynamic, incomplete, and highly size-dispersed, which causes the shift toward a larger R_h and the broadening of the peak shape. At medium concentrations, the C_{18} long carbon chains aggregate to form

hydrophobic cores, while the EO chains are hydrated to form hydrophilic shells, resulting in the formation of stable micelles. Accordingly, the peak becomes sharper and more intense. At high concentrations, the number density of micelles increases and the available space per micelle decreases. Multiple micelles are extruded and merge into larger micelles to reduce the packing repulsion energy, which leads to the decrease in the intensity of the main peak and the broadening of the peak shape in the high-concentration region [32].

3.4. Foam Properties

As illustrated in Fig. 9, a comparison between subplots (a) and (b) reveals that when the concentration is ≤ 1 g/L, the foaming volume of 3SiP2OPA and 2SiP2OPA remains stable above 150 mL after 1000 s; when the concentration exceeds 1 g/L, the foaming volume of 3SiP2OPA and 2SiP2OPA stabilizes within the range of 140-150 mL and above after 1000 s. As presented in subplot (c), the foaming volume of 1227 shows a continuous cliff-shaped decline. As demonstrated in subplots (d) and (e), when the concentration ranges from 0.5 g/L to 1 g/L, the foaming volume of 3SiP5OPA and 2SiP5OPA remains stable above 150 mL after 1000 s, whereas the foaming volume at all other concentrations exhibits a sustained downward trend.

As illustrated in Fig. 10 and Fig. 11, with an increase in concentration, the initial foam generated by 3SiP2OPA, 2SiP2OPA, 3SiP5OPA, 2SiP5OPA and 1227 exhibits higher foam density, smaller individual bubble size, and a larger number of bubbles per unit volume. (Data for the remaining concentrations are provided in Supporting

Information S11-S12) Over the same elapsed duration, 1227 undergoes a greater change in bubble size and ultimately forms larger bubbles. When the concentration exceeds 1 g/L, the residual foam volume of 1227 at 600 s is already far lower than that of 3SiP2OPA, 2SiP2OPA, 3SiP5OPA, and 2SiP5OPA. At 1000 s, no residual foam remains for 1227, while 3SiP2OPA, 2SiP2OPA and 2SiP5OPA still retain substantial amounts of foam, and 3SiP5OPA retains a small volume of foam.The comprehensive evaluation of foam stability performed in this work demonstrates that 3SiP2OPA and 2SiP2OPA exhibit the optimal foaming performance, followed by 3SiP5OPA and 2SiP5OPA, while 1227 shows the poorest foaming performance.

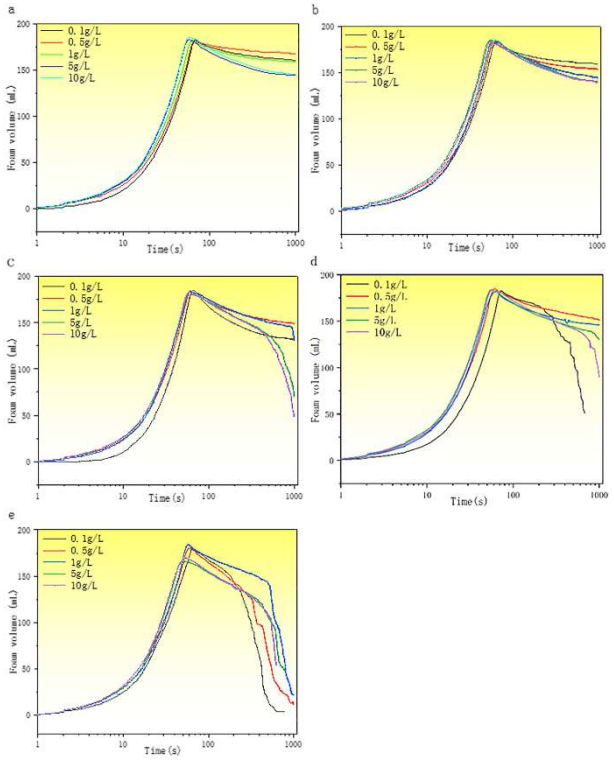


Fig. 9. Variation of foam height as a function of time at different concentrations. (a) 3SiP2OPA, (b) 2SiP2OPA, (c) 3SiP5OPA, (d) 2SiP5OPA, (e) 1227

Foam stability cannot be attained without the contribution of the Gibbs-Marangoni effect [22]. This effect constitutes an intrinsic self-healing mechanism, the efficiency

of which is inherently correlated with the molecular structure of surfactants. Triggered by local thinning of the foam film, the effect induces a surface tension gradient that drives the migration of surface-active substances and bulk liquid flow to repair the thin, fragile regions of the foam film. The key governing parameter in this process is the interfacial diffusion coefficient.There are two primary reasons why 3SiP2OPA, 2SiP2OPA, 3SiP5OPA and 2SiP5OPA exhibit higher foam stability than 1227. First, in contrast to 1227, which contains only one C_{12} long alkyl chain, all four aforementioned compounds possess a C_{18} long alkyl chain, endowing them with a larger dilatational modulus and consequently superior foam stability. Second, unlike 1227, the four target compounds all contain flexible ethylene oxide (EO) chains. The synergistic effect of these two structural features reduces the interfacial diffusion coefficient of 3SiP2OPA, 2SiP2OPA, 3SiP5OPA and 2SiP5OPA, enhances their Gibbs-Marangoni self-healing capacity, and effectively suppresses bubble coalescence [33]. As the bulk concentration of surfactant increases, the foam stability of all five compounds shows a consistent downward trend. This observed behavior can be rationalized by the competitive equilibrium between interfacial adsorption and bulk-phase micellization. With increasing surfactant concentration, this fundamental self-healing mechanism is significantly impaired by micellization: the formation of a large number of micelles depletes the reservoir of free surfactant monomers available for rapid interfacial adsorption. As a result, the replenishment of surfactants to the interface is kinetically hindered, which weakens the Marangoni restoring flow and ultimately leads to foam destabilization.The synthesized product exhibits excellent foam stability and descaling

performance. Therefore, this product is expected to find broad applications in multiple fields including detergent formulation, fire extinguishing and froth flotation [34, 35], where it can improve cleaning efficiency and optimize industrial processing.

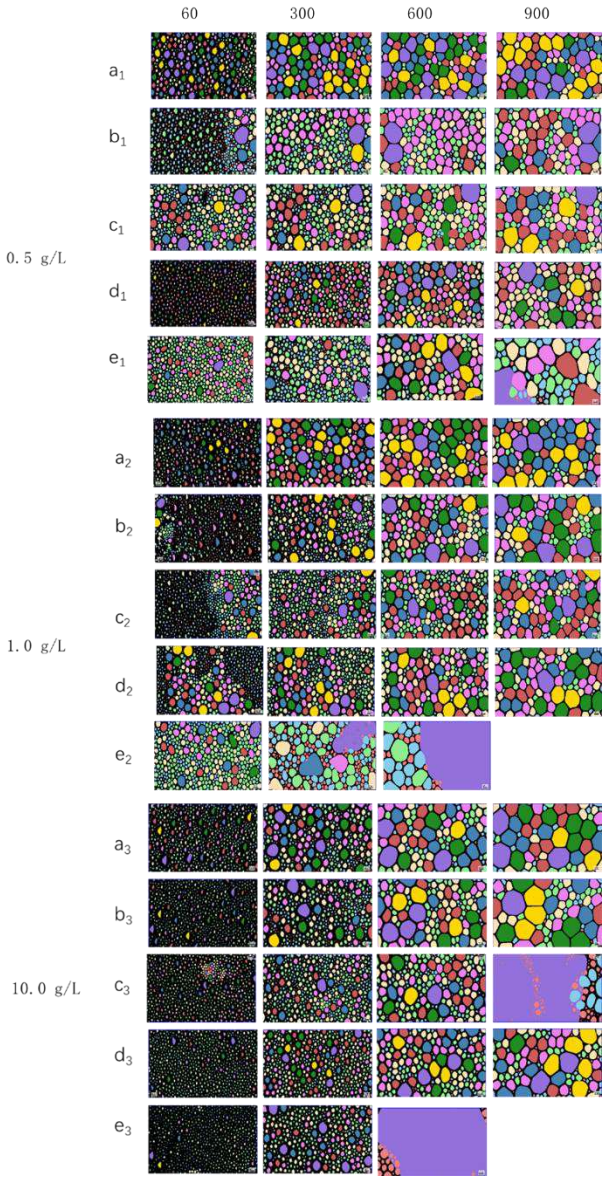


Fig. 10. Photographs of the foams and the distribution at different concentrations. (a_n) 3SiP2OPA, (b_n) 2SiP2OPA, (c_n) 3SiP5OPA, (d_n) 2SiP5OPA, (e_n) 1227 (n=1-3)

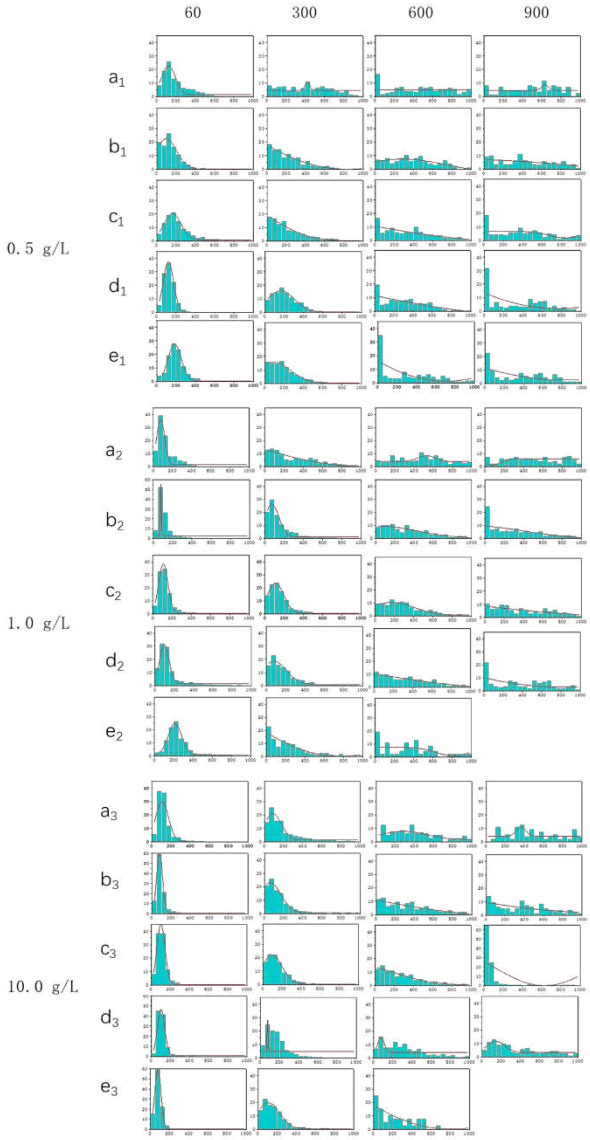


Fig. 11. Histograms of bubble size distributions at different concentrations. (a_n) 3SiP2OPA, (b_n) 2SiP2OPA, (c_n) 3SiP5OPA, (d_n) 2SiP5OPA, (e_n) 1227 (n=1-3)

3.5. Testing on the Long-term Wetting and Spreading Performance of Modified Corn Starch-based Degradable Materials

Wetting and spreading performance is a crucial indicator characterizing the surface properties of materials, and its level directly determines the waterproofing, antifouling, and self-cleaning capacities of materials. The contact angle is a widely adopted parameter for quantifying the wetting and spreading capability of material surfaces, and

its magnitude reflects the interaction strength between liquid and solid interfaces. Measuring the contact angle of droplets on modified materials can directly characterize the spreading performance of the modified substrates. With the development of the modern catering industry, takeaway food has become an indispensable part of people's daily life, and takeaway food containers—especially those fabricated from corn starch-based degradable materials—play an indispensable role in this sector. After hydrophobization modification, starch-based food containers exhibit excessively high contact angles, which brings challenges to subsequent ink printing and label adhesion. Therefore, targeted modification of these materials is required to appropriately reduce their water contact angles and endow the materials with long-term performance stability, so as to facilitate the ink printing and labeling processes of food containers and ensure the firm adhesion of labels and printing ink.

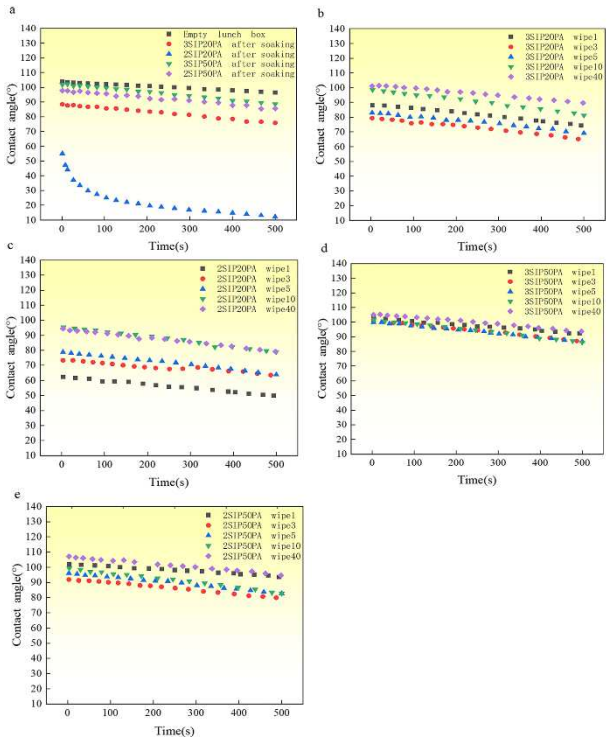


Fig. 12. (a) Contact angle variation curves measured after drying of food containers soaked in

solutions of 3SiP2OPA, 2SiP2OPA, 3SiP5OPA and 2SiP5OPA, (b) Contact angle variation curves measured after drying of food containers subjected to different wiping times after soaking in 3SiP2OPA solution, (c) Contact angle variation curves measured after drying of food containers subjected to different wiping times after soaking in 2SiP2OPA solution, (d) Contact angle variation curves measured after drying of food containers subjected to different wiping times after soaking in 3SiP5OPA solution, (e) Contact angle variation curves measured after drying of food containers subjected to different wiping times after soaking in 2SiP5OPA solution

As illustrated in Fig. 12a, the distilled water contact angle of the blank untreated food container sample was 96.33°. The contact angles of food containers modified with 3SiP2OPA, 3SiP5OPA and 2SiP5OPA were 75.89°, 88.56° and 85.67°, respectively. For 2SiP2OPA-modified samples, the contact angle decreased sharply from the initial value of 55.08° to 29.86° within 60 seconds, and ultimately dropped to 13.13°, confirming that the material surface transformed from hydrophobic to hydrophilic. It can be observed from Fig. 12b–e that the contact angle of each sample after immersion is generally consistent with that measured after one scrubbing cycle. For the same sample, the contact angle remains comparable as the number of scrubbing cycles increases. The observed measurement deviation arises from incomplete drying of the sample prior to testing after scrubbing. Furthermore, even after 40 scrubbing cycles, the contact angles of 2SiP2OPA and 2SiP5OPA still remain lower than that of the blank sample. For 3SiP2OPA and 3SiP5OPA, their contact angles are lower than that of the blank sample after 10 scrubbing cycles. These results demonstrate that the material surface can be converted from hydrophobicity to hydrophilicity with excellent durability, which can be attributed to three main factors:1. The long C18 hydrophobic tail forms a dense adsorption layer on the hydrophobic solid surface; 2. Abundant hydrogen bonds formed between EO chains and water molecules stabilize the hydration

shell; 3. A low critical micelle concentration (CMC) is generally correlated with a more stable micelle structure and slower dissociation kinetics [36] , which allows bulk micelles to continuously release monomers when local desorption or shear expansion occurs at the interface, preventing an instantaneous increase in interfacial tension.The combined effect of these three factors endows the material surface with excellent long-term wettability. Additionally, 2SiP2/5OPA exhibits superior long-term wetting performance compared to 3SiP2/5OPA. This is because 3SiP2/5OPA has one additional highly reactive trimethoxysilane group (Si-O-CH_3) at the molecular terminal relative to 2SiP2/5OPA. When exposed to trace water introduced during scrubbing, this group hydrolyzes and condenses to form Si-OH, which then condenses with the surface hydroxyl groups of the wiping material to form stable covalent bonds. This process leads to the transfer of the anchoring layer and the damage of the hydrophilic protective layer [36, 37]. For the observation that 2/3SiP2OPA exhibits smaller contact angles than 2/3SiP5OPA, this can be explained by the fact that as the number of EO units increases, the EO chain becomes longer. The longer polyoxyethylene head group introduces greater steric repulsion within the adsorption layer, which hinders the close packing of surfactant molecules. This reduces the "effective coverage" of the polar layer at the interface and impairs wettability, which is macroscopically manifested as a contact angle that increases with the increasing number of EO units [28].

3.6. Softness Test

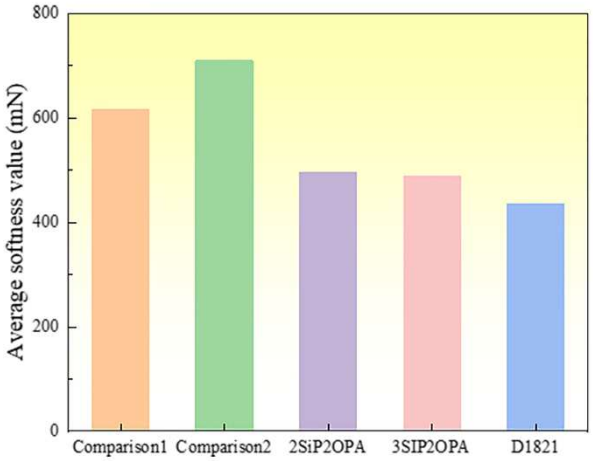


Fig. 13. Average softness values of different samples (Comparison 1: standard detergent; Comparison 2: standard liquid detergent)

Dioctadecyldimethylammonium chloride (D1821) is an irreplaceable cost-effective primary raw material in the fields of fabric softeners and textile finishing in the Chinese market, and thus it was selected as the control sample in this study. The results of the softness test (Fig. 13) demonstrate that the softness performance of the tested samples outperforms that of the standard detergent, and the softness value of 3/2SiP2OPA is close to that of D1821. The softness ratio P of the three samples relative to the standard detergent was calculated: the P values of 2SiP2OPA against the two standard detergents are 1.25 and 1.43 respectively, and the P values of 3SiP2OPA against the two standard detergents are 1.26 and 1.45 respectively. The calculation results indicate that both products possess softening performance, which originates from the directional surface adsorption of the amphiphilic structure of the samples: the long linear C18 hydrophobic tails form a flexible and shearable hydrophobic lubricating layer on the fiber surface (the intramolecular rotation of C-C single bonds endows the layer with flexibility), while the polyoxyethylene head groups maintain hydrophilic

compatibility with the system; this effect significantly reduces the static friction coefficient μ_s between fibers, thereby endowing the fabric with a soft, fluffy and smooth handfeel [38].

3.7. Long-lasting Antistatic Property Test on Polyurethane Fabric

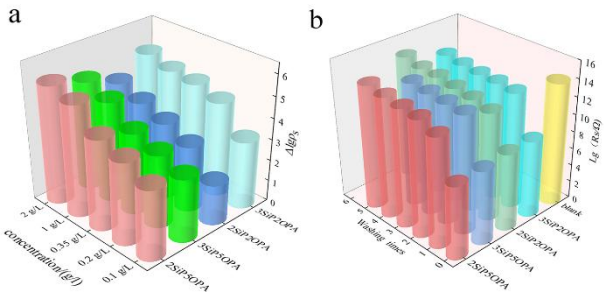


Fig. 14. (a) Antistatic performance of samples with different concentrations; (b) Long-term durability of antistatic performance for different samples at a concentration of 10 g/L

Quaternary ammonium salt surfactants carry positive charges and thus can adsorb onto fabric surfaces via electrostatic interactions, effectively reducing the accumulation of static electricity on fabric surfaces. The logarithmic attenuation value ΔlgρS of the sample is calculated based on the measured surface resistance (RS) obtained from the instrument, to evaluate the antistatic performance of the sample. Polyurethane fabric materials are widely used in outdoor jackets, raincoats, mountaineering clothing and various protective workwear due to their excellent water resistance, wind resistance and abrasion resistance [39]. However, most of these materials use insulating fibers such as polyester or nylon as the base fabric, and the polyurethane coating forms a dense high - resistance layer, resulting in a surface resistance of the fabric that is often $\geq 10^{12}$ Ω. In dry or low - humidity environments, static charge is easily accumulated during friction, clothing undressing and winding processes, leading to issues such as dust adsorption

and electric shock discomfort. In flammable environments containing oil and gas or dust, there is a risk of ignition caused by electrostatic discharge, and electrostatic accumulation may interfere with the operation and accuracy of devices in scenarios with dense electronic equipment [40]. Therefore, conducting long-lasting antistatic modification on polyurethane fabrics has clear practical necessity.

Fig. 14a shows that among different samples at the same concentration, 2SiP5OPA exhibits the maximum ΔlgρS and delivers the best antistatic performance. As the concentration increases, the antistatic performance of the samples first increases and then tends to stabilize. Increased concentration promotes the adsorption and deposition of quaternary ammonium salts on fabric surfaces, effectively inhibiting the generation and accumulation of static electricity. When the adsorption capacity reaches saturation, the surfactant no longer continues to adsorb. After the adsorption capacity of the fabric surface is saturated, the large steric hindrance of long-carbon-chain silane limits the migration rate of ions, leading to a reduction in charge dissipation efficiency. Fig. 14b shows that 2SiP5OPA, 2SiP2OPA, 3SiP5OPA and 3SiP2OPA require 6, 7, 5 and 6 washing cycles respectively for their lgR/Ω values to reach the same level as that of the blank sample. In addition, 2SiP2/5OPA demonstrates better long - lasting antistatic performance than 3SiP2/5OPA. The reason is that 3SiP2/5OPA has one more highly reactive silmethoxy group (Si-O-CH_3) at the molecular terminal than 2SiP2/5OPA. Trace water present during the scrubbing process of the treated material surface hydrolyzes Si-O-CH_3 into Si-OH upon contact, which then condenses with hydroxyl groups on the surface of the wiping object to form stable covalent bonds, resulting in

the transfer of the anchoring layer and damage to the wetting protective layer. Among the tested samples, 2SiP2OPA and 3SiP2OPA exhibit stronger long - lasting antistatic performance than 2SiP5OPA and 3SiP5OPA. There are four main reasons for this performance difference: 1. The lipophilic C_{18} tails are embedded toward the matrix side, while the hydrophilic EO chains extend toward the air side. After oriented arrangement, a continuous/quasi-continuous polar layer is formed on the outer surface; 2. The polymerized EO segments have good hygroscopicity, which facilitates the formation of ionic conductive channels; 3. A low critical micelle concentration (CMC) is usually accompanied by a more stable micelle structure and slower dissociation kinetics [36] , which allows bulk micelles to continuously release monomers when local desorption or shear expansion occurs at the interface; 4. As the number of EO units increases, the anchoring ratio of C_{18} (hydrophobic/hydrophilic ratio) decreases, leading to the degradation of the oriented surface adsorption layer and ultimately resulting in an unstable conductive film. The synergistic effect of these four factors endows the samples with excellent long-lasting antistatic performance [41].

3.8. Long-lasting Antibacterial Performance Test on Polyurethane Fabric

3.8.1. Oscillation Method

The oscillation method is mainly used to evaluate the antibacterial performance of antibacterial materials. This method simulates a dynamic environment through physical oscillation to accelerate the contact between bacteria and antibacterial agents, so that it can reflect the actual antibacterial effect more accurately. The oscillation method can

be applied to test the long-term antibacterial performance of antibacterial materials on fabrics. The long-term antibacterial performance and stability of the samples were verified through four repeated experiments. After the completion of each experiment, the fabric samples were washed, dried and stored for 2 months before being used for the next round of experiments.

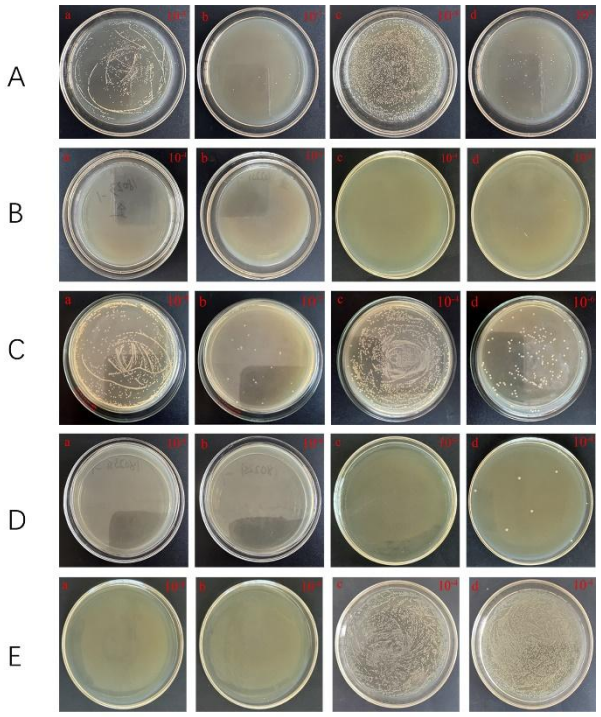


Fig. 15. (A)Staphylococcus aureus in blank control (a, b) and "zero-contact" control (c, d), (B)Staphylococcus aureus cultured on 0-wash (a/b) and 30-wash (c/d) 3/2SIP2OPA samples, (C) Escherichia coli in blank control (a, b) and "zero-contact" control (c, d), (D) Escherichia coli cultured on 0-wash (a/b) and 30-wash (c/d) 3/2SIP2OPA samples, (E) Staphylococcus aureus on 30-wash (a/b) 3/2SIP5OPA samples and Escherichia coli cultured on 5-wash (c/d) 3/2SIP5OPA. samples

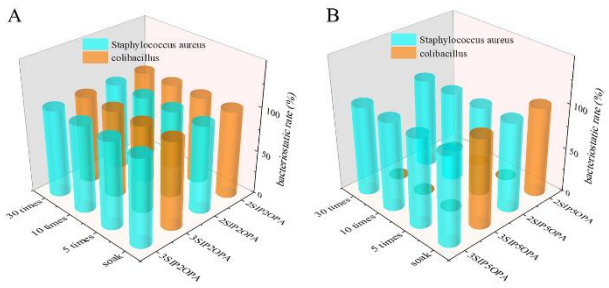


Fig. 16. (A) Bacteriostatic rates of the 3/2SIP2OPA sample after different cycles of immersion and washing, (B) Bacteriostatic rates of the 3/2SIP5OPA sample after different cycles of immersion and washing

Fig. 15 and Fig. 16 demonstrate that the fabrics grafted onto the samples exhibit inhibitory effects on the growth of both tested bacterial strains. Even after 30 washing cycles, 3/2SIP2OPA still maintains excellent antibacterial performance against Staphylococcus aureus and Escherichia coli, with the bacterial inhibition rate remaining no less than 99.9%. In contrast, the antibacterial activity of 3/2SIP5OPA against S. aureus and E. coli changes considerably: after 30 washing cycles, 3/2SIP5OPA still retains a bacterial inhibition rate of no less than 99.9% against S. aureus, but its inhibition rate against E. coli drops to zero after only 5 washing cycles. This difference can be attributed to the following factors: 1. The positive charge of quaternary ammonium salt binds to the negative charge on the bacterial membrane surface via electrostatic interaction, neutralizing the charge barrier. The C_{18} long hydrophobic chain inserts into the phospholipid bilayer, triggering the disruption of membrane lipid order and increasing membrane permeability, ultimately leading to bacterial death [42, 43]; 2. The low critical micelle concentration (CMC) of the sample endows its monomers with higher relative reactivity and greater membrane insertion efficiency, thereby resulting in better antibacterial performance; 3. A lower polymerization degree of

ethylene oxide (EO) drives the overall hydrophilic-hydrophobic balance (HLB) of the sample molecule to favor hydrophobicity, which facilitates insertion into membrane lipids [22]; 4. The binding between the sample and the fabric surface involves three interaction modes: physical adsorption, chemical bonding and van der Waals force. Samples with three methoxy groups bind more strongly to the fabric than those with two methoxy groups. Therefore, 3/2SIP2OPA possesses excellent long-lasting antibacterial activity, highlighting its unique advantage of sustained effectiveness in practical applications.

3.8.2. Microscopic Morphology

Via scanning electron microscopy surface morphology analysis (Fig. 17), no significant morphological differences were observed between treated and untreated fabrics. This indicates that the test sample does not alter the macroscopic morphology of the fabric. Theoretically, silicon elements in the sample can undergo covalent condensation with hydroxyl groups on the fabric surface. We used scanning electron microscopy for energy-dispersive spectroscopy mapping to characterize the distribution of nitrogen and silicon elements on the fabric, and further verified the loading stability via changes in the silicon mass fraction. Untreated fabrics inherently contain a low background content of silicon; after impregnation with the test sample, the silicon content of the fabric increased notably. After 15 washing cycles, the silicon content decreased slightly, but still remained significantly higher than that of untreated fabric. These results confirm that the test sample can stably adhere to and remain on the fabric surface after multiple washing cycles.

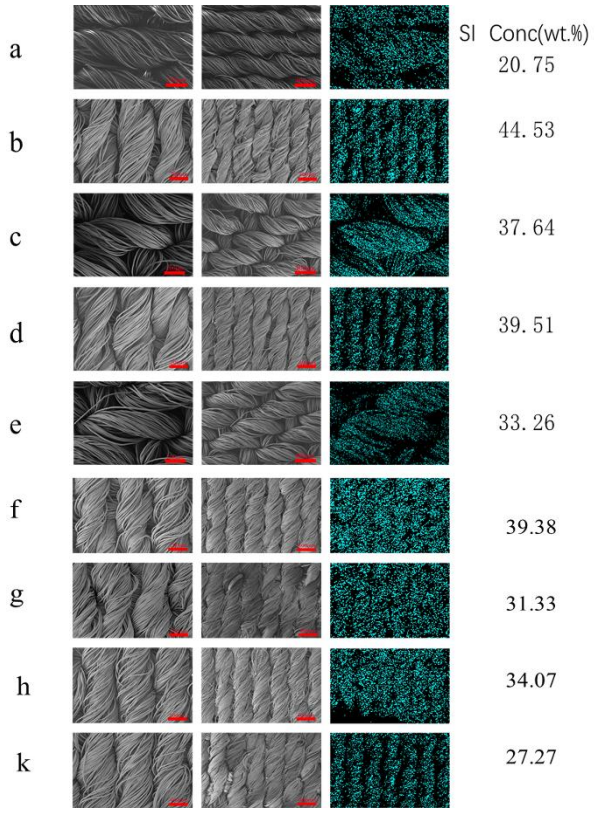


Fig. 17. Scanning electron microscopy images of fabric samples: (a) untreated fabric, (b) 3SIP2OPA after impregnation, (c) 3SIP2OPA after impregnation and 15 cycles of cleaning, (d) 2SIP2OPA after impregnation, (e) 2SIP2OPA after impregnation and 15 cycles of cleaning, (f) 3SIP5OPA after impregnation, (g) 3SIP5OPA after impregnation and 20 cycles of cleaning, (h) 2SIP5OPA after impregnation, (k) 2SIP5OPA after impregnation and 20 cycles of cleaning.

Via AFM imaging (Fig. 18), the adsorption morphologies of the blank, 2SiP2/5OPA and 3SiP2/5OPA samples on the fabric surface can be observed. Table 2 presents the average surface roughness (Ra), root mean square roughness (Rq) and maximum height roughness (Rmax) of the fabric surfaces for the untreated group, the groups immersed in 2SiP2/5OPA and 3SiP2/5OPA samples, and the groups subjected to 15 washing cycles after immersion. AFM micrographs demonstrate that the samples adsorb onto the fabric in a granular morphology. The Ra and Rq values of the fabrics after sample immersion and after 15 washing cycles following immersion are higher than those of the untreated fabric. For 2/3SiP2OPA samples, the Rmax value changes

from the initial 326 to 896/1850 after immersion, and to 449/693 after 15 washing cycles following immersion; for 2/3SiP5OPA samples, the Rmax value changes from the initial 326 to 833/671 after immersion, and to 388/545after 20 washing cycles following immersion. These results indicate that the adhesion of the samples to the fabric increases the surface adsorption capacity; after multiple washing cycles, the surface adsorption capacity decreases but remains significantly higher than that of the original fabric, which verifies that the effect of the samples persists after washing the fabric.

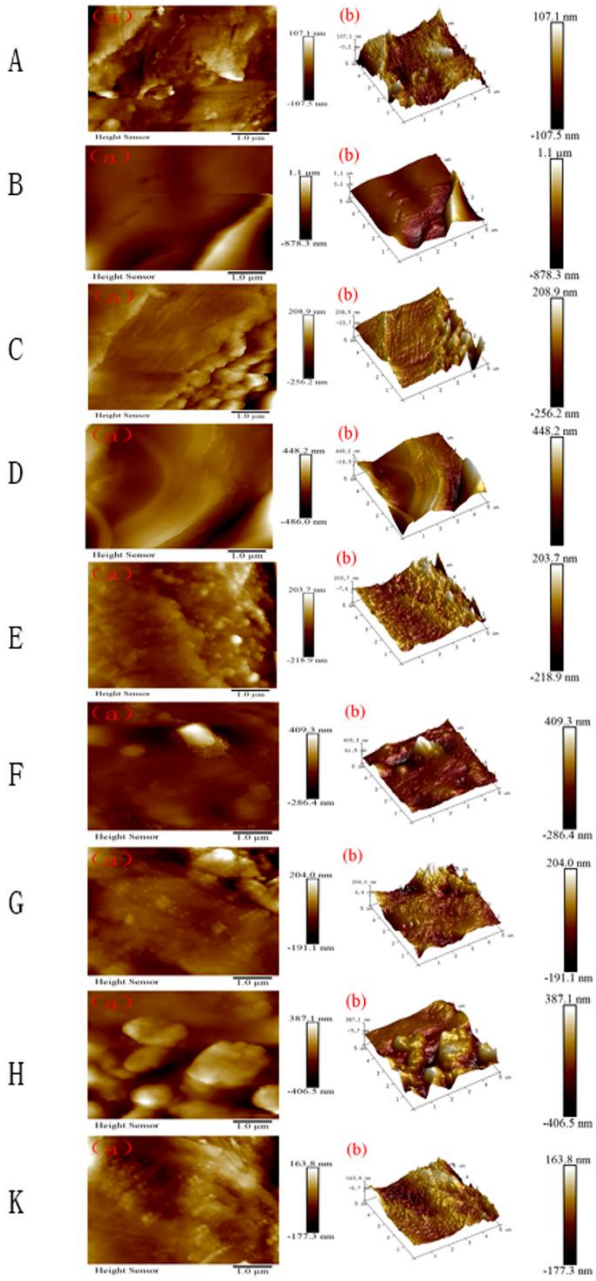


Fig. 18. (a) AFM images and (b) 3D images of the fabric samples. (A) Untreated fabric specimen, (B) Fabric specimen after immersion in 3SiP2OPA, (C) Fabric specimen after immersion in 3SiP2OPA and 15 cycles of washing, (D) Fabric specimen after immersion in 2SiP2OPA,(E) Fabric specimen after immersion in 2SiP2OPA and 15 cycles of washing, (F) Fabric specimen after immersion in 3SiP5OPA, (G) Fabric specimen after immersion in 3SiP5OPA and 20 cycles of washing, (H) Fabric specimen after immersion in 2SiP5OPA, (K) Fabric specimen after immersion in 2SiP5OPA and 20 cycles of washing.

Table 2 Surface Roughness

Sample Name	Ra/(nm)	Rq/(nm)	Rmax/(nm)
Untreated Sample Fabric Sheet	23.8	30.2	326
Immersed in 3SiP2OPA Fabric Sheet	153	226	1850
Immersed in 3SiP2OPA after 15 Washing Cycles Fabric Sheet	32.5	49.7	693
Immersed in 2SiP2OPA Fabric Sheet	91.7	118	896
Immersed in 2SiP2OPA after 15 Washing Cycles Fabric Sheet	37.4	49.9	449
Immersed in 3SiP5OPA Fabric Sheet	40.5	66.3	671
Immersed in 3SiP5OPA after 20 Washing Cycles Fabric Sheet	31.2	45.0	545
Immersed in 2SiP5OPA Fabric Sheet	83.3	110	833
Immersed in 2SiP5OPA after 20 Washing Cycles	33.5	44.6	388

3.8.3. Skin Irritation and Acute Oral Toxicity

Table 3 Results of the Skin Irritation Assay for 3SIP2OPA

Number	Weight	Group	Signs	Contact time		
				1h	24h	48h
1	2.12kg	Experimental	Erythema	0	0	0
			Dropsy	0	0	0
		Control	Erythema	0	0	0
			Dropsy	0	0	0
2	2.21kg	Experimental	Erythema	0	0	0
			Dropsy	0	0	0
		Control	Erythema	0	0	0
			Dropsy	0	0	0
3	2.18kg	Experimental	Erythema	1	1	1
			Dropsy	0	0	0
		Control	Erythema	0	0	0
			Dropsy	0	0	0

Table 3 summarizes the results of in vivo rabbit skin irritation tests, with detailed supporting information provided in Section S13. The results confirm that the 3SIP2OPA sample is non-irritating to skin, with an irritation score of 0.33. Among the three female

experimental rabbits, only one individual developed erythema within 1 hour to 2 days post-exposure, and no edema was observed in any subject. These findings demonstrate that 3SIP2OPA can be used as a non-irritating fabric finishing agent, making it suitable for high-frequency skin contact scenarios and long-term use by individuals with sensitive skin.

Table 4 Results of the Acute Oral Toxicity Test of SIP2OPA

Sex	Amount of gavage (ml/kg · BW)	The number of animals	Average weight (g)			The number of deaths	LD50 (mg/kg · BW)
			Day 1	Day 7	Day 14		
Male	5000	10	19.9± 0.63	29.0±1.25	38.4±1.90	0	>5000
Female	5000	10	18.9± 0.57	26.8±1.42	33.0±2.02	0	>5000

Table 4 presents the results of the acute oral toxicity test (Supporting Information S14), indicating that the 3SIP2OPA sample is practically non-toxic in acute oral toxicity assays. First, all 20 rats (10 males and 10 females) in the treatment group survived the 14-day observation period without exhibiting toxic symptoms such as convulsions, diarrhea, or dyspnea. Second, no abnormal histomorphology of organs or histopathological changes were observed in necropsy. Third, based on the criterion that a lethal dose 50 (LD_{50}) exceeding 5000 mg/kg body weight indicates non-toxicity, the safety of 3SIP2OPA was confirmed to be significantly superior to that of traditional quaternary ammonium disinfectants. There are three main reasons for the non-toxicity and non-irritation of the sample: 1. The excessively long carbon chain of 3SIP2OPA dramatically increases the non-polarity of the molecule, rendering this ultra-long

molecule extremely difficult to dissolve in aqueous media (i.e., blood). Meanwhile, due to its large molecular size, it cannot effectively penetrate the lipid bilayer of cell membranes [22]; 2. The hydrophilic headgroup composed of ethylene oxide (EO) chains on the sample limits the depth of membrane penetration [44]; 3. The hydrolyzable Si-O-CH_3 moiety in the organosilicon group generates Si-OH structures, which undergo dehydration condensation to form siloxane chains. Through weak hydrogen bonding interactions with skin keratin, this structure avoids the dissolution of membrane lipids caused by traditional disinfectants and forms a protective layer on the skin surface [45, 46].

4. Conclusion

This study addresses a long-standing "triple dilemma" that constrains the development of high-performance functional surfaces: the inability to simultaneously achieve durable bacteriostasis, durable wettability and durable antistatic properties within a single coating system. To resolve this dilemma, this study successfully synthesized four novel polyether-modified organosilicon quaternary ammonium salts (2/3SiP2/5OPA) via a one-step quaternization method, and systematically clarified the intrinsic correlation between their molecular structure, aggregation morphology, interfacial properties, and long-acting performance. The results demonstrate that this class of surfactants exhibits excellent surface activity: the critical micelle concentration (CMC) of 3SiP2OPA is as low as 0.0031 g/L, and the minimum equilibrium surface tension at cmc (γCMC) of 2SiP2OPA reaches 37.62 mN/m. Furthermore, the self-assembly behavior of these compounds can be precisely regulated by the length of

hydrophobic chains: 2/3SiP2OPA and 2/3SiP5OPA respectively present the characteristics of nanoscale bimodal distribution of vesicles and spherical micelles. More importantly, confirmed by SEM/AFM characterization, the target products can form chemical bonds with the substrate surface, which enables this series of products to achieve a breakthrough in functional extension compared with conventional products. After modifying the surface of corn starch-based materials and polyurethane fabrics with 2SiP2/5OPA and 3SiP2/5OPA, the modified materials are endowed with multiple long-lasting properties: 2SiP2/5OPA retains effectiveness after up to 40 scrub cycles for persistent wettability; 2SiP2OPA retains effectiveness after up to 7 washing cycles for persistent antistatic performance; and the antibacterial rate of 2/3SiP2OPA against Staphylococcus aureus and Escherichia coli still remains above 99.9% after 30 washing cycles for persistent antibacterial activity. Rabbit skin irritation tests and mouse oral toxicity tests verify that 3SiP2OPA is non-toxic and non-irritating.In conclusion, compared with the 2/3SiP5OPA series, the 2/3SiP2OPA series delivers superior performance in both physicochemical properties and application performance. Through a distinctive structure regulation strategy, this class of polyether organosilicon quaternary ammonium salts successfully addresses the industrial pain points of existing disinfectant products, namely single functionality and poor durability. Integrating long-acting antibacterial, antistatic, wetting and softening properties into a single molecule, this product shows remarkable industrialization potential and application value in functional coatings, biodegradable materials, high-end medical textiles and other fields.

CRediT authorship contribution statement

Linfei Li: Data curation, Investigation, Resources, Writing-original draft. Ran Wei: Investigation.Yimeng Zhao: Investigation.Lifei Zhi: Resources, Validation, Writing-review & editing. Guoyong Wang: Resources, Investigation. Yongqiang Sun: Resources, Validation.

Data availability

All relevant data are within the paper. Data will be made available on request.

Declaration of interests

The authors declare that they have no known competing financial interests or personal relationships that could have appeared to influence the work reported in this paper.

Acknowledgments

We acknowledge with gratitude the policy support from the General Office of the Ministry of Industry and Information Technology of the People's Republic of China for the issuance of the "One-stop" Application Plan for Key Products and Processes for 2025.

Funding

This reearch was supported by the Fundamental Research Program of Shanxi Province (No. 202403021221145).

Ethics declaration

The oral toxicity assays performed on mice in this study were conducted in

accordance with ethical guidelines (2025SP14849R01) .

References

[1] Falk N A. Surfactants as antimicrobials: a brief overview of microbial interfacial chemistry and surfactant antimicrobial activity, J. Surfactants Deterg. 22(5)(2019)1119-1127, https://doi.org/10.1002/jsde.12293.

[2] Zhou C, Wang Y. Structure–activity relationship of cationic surfactants as antimicrobial agents, Curr Opin Colloid In. 45(2020)28-43, https://doi.org/10.1016/j.cocis.2019.11.009.

[3] Nadagouda, Mallikarjuna N., et al. Antimicrobial activity of quaternary ammonium salts: structure-activity relationship, Med. Chem. Res. 31(10)(2022) 1663-1678, https://doi.org/10.1007/s00044-022-02924-9.

[4] Meng X, Wang Y, Wang J, et al. The Synthesis of Novel Glucosylamide Organosilicon Quaternary Ammonium Salts and Long-Lasting Modification of Different Materials, Molecules. 30(19)(2025)3934, https://doi.org/10.3390/molecules30193934.

[5] Luengo G S, Aubrun O, Restagno F. Foams in cosmetics: New trends in detergency, friction, coatings, Curr Opin Colloid In. 77(2025)101906, https://doi.org/10.1016/j.cocis.2025.101906.

[6] Wang, Yu, et al. An environmentally friendly coating: Excellent self-cleaning, efficient antimicrobial, and durability properties, Surf. Interfaces. 53(2024) 105053, https://doi.org/10.1016/j.surfin.2024.105053.

[7] Ezelarab HAA, Abbas SH, Abourehab MAS, et al. Novel anti-microbial ciprofloxacin-pyridinium quaternary ammonium salts with improved

physicochemical properties and DNA gyrase inhibitory activity, Med Chem Res. 30 (12)(2021)2168–83, https://doi.org/10.1007/s00044-021-02798-3.

[8] Gonçalves R A, Holmberg K, Lindman B. Cationic surfactants: A review, J. Mol. Liq. 375(2023)121335, https://doi.org/10.1016/j.molliq.2023.121335.

[9] Zakharova, Lucia Ya, et al. Cationic surfactants: Self-assembly, structure-activity correlation and their biological applications, Int. J. Mol. Sci. 20(22)(2019)5534, https://doi.org/10.3390/ijms20225534.

[10] Sharma, Pradyumn, et al. Interactions of surfactants with the bacterial cell wall and inner membrane: Revealing the link between aggregation and antimicrobial activity, Langmuir. 38(50)(2022)15714-15728, https://doi.org/10.1021/acs.langmuir.2c02520.

[11] Hassabo A G, Saad F, Hegazy B M, et al. The use of cationic surfactants in the textiles industry, J. Text. Color. Polym. Sci. 20(2)(2023)227-242, https://doi.org/10.21608/jtcps.2023.216820.1189.

[12] Wang J, Wang Y, Zheng Y, et al. Study on the long-term modification of fabric surface by novel glycosylamide organosilicones quaternary ammonium salts, Prog. Org. Coat. 210(2026)109640, https://doi.org/10.1016/j.porgcoat.2025.109640.

[13] Levine, Lauren B, et al. Solvent-free surface engineering of LiNi0. 6Mn0. 2Co0. 2O2 using a hydrophobic fluorosilane to enhance moisture stability, Surf. Interfaces. (2026)110200, 10.1016/j.surfin.2026.110200.

[14] Sayed SRM, Ezzat AO, Yassin MT, et al. Synthesis, characterization and application of novel cationic surfactants as antibacterial agents, Separations. 10(2)(2023)97, https://doi.org/10.3390/separations10020097.

[15] Dou J, Liu J, Wang Y, et al. Surface activity, wetting, and aggregation of a

perfluoropolyether quaternary ammonium salt surfactant with a hydroxyethyl group, Molecules. 28(20)(2023)7151, https://doi.org/10.3390/molecules28207151.

[16] Ram-On M, Cohen Y, Talmon Y. Effect of polyelectrolyte stiffness and solution pH on the nanostructure of complexes formed by cationic amphiphiles and negatively charged polyelectrolytes, J. Phys. Chem. B. 120(26)(2016): 5907-5915, https://doi.org/10.1021/acs.jpcb.6b01138.

[17] Matthew, L.L. Tom, K. Michael, R.W. Anticipating colloidal instabilities in cationic vesicle dispersions by measuring collective motions with dynamic light scattering, J. Colloid Interface Sci. 296(2006)599–607, https://doi.org/10.1016/j.jcis.2005.09.048.

[18] Milad, E. Karin, S. Stoyan, I. Nikolay, G. Kerstin, E. Oppositely charged surfactants and nanoparticles at the air-water interface:Influence of surfactant to nanoparticle ratio, J. Colloid Interface Sci. 653(2024)1388–1401, https://doi.org/10.1016/j.jcis.2023.09.038.

[19] Ning, B. Zhang, M. Bai, Y. Wang, W. Wang, G. Comparison of the properties of perfluoroalkyl polyoxyethylene ether and alkyl polyoxyethylene ether, Colloid Polym. Sci. 298(10)(2020)1389–1399, https://doi.org/10.1007/s00396-020-04732-2.

[20] Shi, X. Zeng, M. Xu, X. Liu, Y. Kou, J. Bian, Q. Song, H. Zhang, J. Wang, Q. Promotion of droplet deposition, diffusion-wetting and retention on hydrophobic surfaces by nonionic star-shaped oligomeric surfactants, J. Mol. Liq.

386(2023)122521, https://doi.org/10.1016/j.molliq.2023.122521.

[21] Wang Y, Chen Z, Zhang E, et al. Aggregation behavior and application properties of novel glycosylamide quaternary ammonium salts in aqueous solution, Molecules. 29(12)(2024)2749, https://doi.org/10.3390/molecules29122749.

[22] Rosen M.J, Kunjappu J.T. Surfactants and Interfacial Phenomena, John Wiley & Sons. 42(5)(2005)42-2832-42-2832, https://doi.org/10.5860/choice.42-2832.

[23] Sharma R, Mahajan S, Mahajan R.K. Surface adsorption and mixed micelle formation of surface active ionic liquid in cationic surfactants: Conductivity, surface tension, fluorescence and NMR studies, Colloid Surf. A. 427(2013)62–75, https://doi.org/10.1016/j.colsurfa.2013.03.023.

[24] Merchel Piovesan Pereira B, Tagkopoulos I. Benzalkonium chlorides: uses, regulatory status, and microbial resistance, Appl. Environ. Microbiol. 85(13)(2019)e00377-19, https://doi.org/10.1128/aem.00377-19.

[25] Kovač B, Piletić K, Kovačević Ganić N, et al. The effectiveness of benzalkonium chloride as an active compound on selected foodborne pathogens biofilm, Hygiene. 2(4)(2022)226-235, https://doi.org/10.3390/hygiene2040020.

[26] Rincón-Romero J F, Ríos F, Reyes-Requena A, et al. Surface and thermodynamics properties of commercial fatty-alcohol ethoxylate surfactants, J. Mol. Liq. 376(2023)121396, https://doi.org/10.1016/j.molliq.2023.121396.

[27] Jiaolong Q, Wenwen P, Xiaodong Y, et al. Studies on the surface properties of alcohol ethoxylate and the application in suspension concentrate, Chem. J. Chin. Univ. 35(10)(2014)2182-2190, 10.7503/cjcu20140331.

[28] Tyrode E, Johnson C M, Kumpulainen A, et al. Hydration state of nonionic surfactant monolayers at the liquid/vapor interface: Structure determination by vibrational sum frequency spectroscopy, J. Am. Chem. Soc. 127(48)(2005)16848-16859, https://doi.org/10.1021/ja053289z.

[29] Myers D. Surfaces, interfaces, and colloids, New York: Wiley. 1999.

[30] Wang Y, Dou J, Bian Q, Zhi L, Han Z, Wang G. Physicochemical Properties of Polyether-Modified Fluorosilicone Surfactants in Ethanol/Water Mixed Solutions, Langmuir.41(2025)11173–11182, https://doi.org/10.1021/acs.langmuir.5c01000.

[31] Shaban S.M, Fouda A.S, Elmorsi M.A, Fayed T, Azazy O. Adsorption and micellization behavior of synthesized amidoamine cationic surfactants and their biological activity, J. Mol. Liq. 216(2016)284–292, https://doi.org/10.1016/j.molliq.2015.12.111.

[32] Alami E, Almgren M, Brown W, et al. Aggregation of hydrophobically end-capped poly (ethylene oxide) in aqueous solutions. Fluorescence and light-scattering studies, Macromolecules. 29(6)(1996)2229-2243, https://doi.org/10.1021/ma951174h.

[33] Song B L, Zhal Z L, Zhao J X, et al. Interfacial Adsorption, Dilational Visco-Elasticity and Foam Stability in a Mixed System of Gemini Surfactant/C12E n, Acta Phys.-Chim. Sin. 31(12)(2015)2324-2331, 10.3866/PKU.WHXB201510231.

[34] Vinogradov A.V, Kuprin D.S, Abduragimov I.M, Kuprin G.N, Serebriyakov E, Vinogradov V.V. Silica Foams for Fire Prevention and Firefighting, ACS Appl. Mater. Interfaces. 8(2016)294–301, https://doi.org/10.1021/acsami.5b08653.

[35] Bois R, Pezron I, Rotureau P, Van Hecke E, Fayet G, Nesterenko A. Foaming behavior of sugar-based surfactants: Influence of molecular structure and anticipation from surface properties, J. Dispers. Sci. Technol. 44(2023)840–851, https://doi.org/10.1080/01932691.2021.1974877.

[36] Pantelidou M S, García Daza F A, Avalos J B, et al. Universal scaling for the exit dynamics of block copolymers from micelles at short and long time scales, Macromolecules. 55(3)(2022)914-927, https://doi.org/10.1021/acs.macromol.1c02387.

[37] Sambhy V, Peterson B R, Sen A. Multifunctional silane polymers for persistent surface derivatization and their antimicrobial properties, Langmuir. 24(14)(2008)7549-7558, https://doi.org/10.1021/la800858z.

[38] Igarashi T, Nakamura K. Elucidation of the softening mechanism of fabric softeners, J. Text. Eng. Fash. Technol. 2(2)(2017)322-324, 10.15406/jteft.2017.02.00051.

[39] Desai S K, Bera S, Mondal D. Multifaceted synthesis, properties and applications of polyurethanes and its composites, Curr. Org. Chem. 23(4)(2019)361-389, https://doi.org/10.2174/1385272823666190315160000.

[40] Cheremisinoff N P. Dust Explosion and Fire Prevention Handbook: A Guide to Good Industry Practices, John Wiley & Sons. (2014).

[41] Lu Q, Chen Y, Huang J, et al. A directional entrapment modification on the polyethylene surface by the amphiphilic modifier of stearyl-alcohol poly (ethylene oxide) ether, Appl. Surf. Sci. 441(2018)130-137,

https://doi.org/10.1016/j.apsusc.2018.01.300.

[42] Marcotte L, Barbeau J, Lafleur M. Permeability and thermodynamics study of quaternary ammonium surfactants—phosphocholine vesicle system, J. Colloid Interface Sci. 292(1)(2005)219-227, https://doi.org/10.1016/j.jcis.2005.05.060.

[43] Fukahori M, Akatsu S, Sato H, et al. Effects of the structures of polyoxyethylene alkyl ethers on uptake of butyl p-hydroxybenzoate by Escherichia coli and its antibacterial activity, Chem. Pharm. Bull. 44(12)(1996)2335-2337, https://doi.org/10.1248/cpb.44.2335.

[44] Rissanen S, Kumorek M, Martinez-Seara H, et al. Effect of PEGylation on drug entry into lipid bilayer. J. Phys. Chem. B. 118(1)(2014)144-151, https://doi.org/10.1021/jp4105745.

[45] Lin G H Y, Hemming M. Ocular and dermal irritation studies of some quaternary ammonium compounds, Food Chem. Toxicol. 34(2)(1996)177-182, https://doi.org/10.1016/0278-6915(95)00099-2.

[46] Presley C L, Militello M, Barber C, et al. The history of surfactants and review of their allergic and irritant properties, Dermatitis. 32(5)(2021)289-297, https://doi.org/10.1097/der.0000000000000730.

Supplementary Files

This is a list of supplementary files associated with this preprint. Click to download.

- Supplementarymaterial.doc